Open access • Journal Article • DOI:10.1086/338088

HIPASS high-velocity clouds: properties of the compact and extended populations

Mary E. Putman, Mary E. Putman, V. de Heij, Lister Staveley-Smith ...+30 more authors

Institutions: University of Colorado Boulder, Australia Telescope National Facility, ASTRON, Australian National University ...+9 more institutions

Published on: 01 Feb 2002 - The Astronomical Journal (American Astronomical Society)

Topics: HIPASS, Magellanic Stream, High-velocity cloud and Population

The Astronomical Journal, 123:873–891, 2002 February

HIPASS HIGH-VELOCITY CLOUDS: PROPERTIES OF THE COMPACT AND EXTENDED POPULATIONS

M. E. Putman,[1,2,3] V. de Heij,[4] L. Staveley-Smith,[2] R. Braun,[5] K. C. Freeman,[1] B. K. Gibson,[6] W. B. Burton,[4] D. G. Barnes,[6] G. D. Banks,[7] R. Bhathal,[8] W. J. G. de Blok,[2] P. J. Boyce,[7] M. J. Disney,[7] M. J. Drinkwater,[9] R. D. Ekers,[2] P. A. Henning,[10] H. Jerjen,[1] V. A. Kilborn,[11] P. M. Knezek,[12] B. Koribalski,[2] D. F. Malin,[13] M. Marquarding,[2] R. F. Minchin,[7] J. R. Mould,[1] T. Oosterloo,[5] R. M. Price,[10] S. D. Ryder,[13] E. M. Sadler,[14] I. Stewart,[2,15] F. Stootman,[8] R. L. Webster,[9] and A. E. Wright[2]

Received 2001 July 10; accepted 2001 October 10

ABSTRACT

A catalog of southern anomalous-velocity H I clouds at decl. $< +2^\circ$ is presented. This catalog is based on data from the H I Parkes All-Sky Survey (HIPASS) reprocessed with the MINMED5 procedure and searched with a new high-velocity cloud-finding algorithm. The improved sensitivity (5 σ: $\Delta T_B = 0.04$ K), resolution (15.′5), and velocity range (-500 km s^{-1} $< V_{\rm LSR} <$ $+500$ km s^{-1}) of the HIPASS data result in a substantial increase in the number of individual clouds (1956, as well as 41 galaxies) compared with what was known from earlier southern data. The method of cataloging the anomalous-velocity objects is described, and a catalog of key cloud parameters, including velocity, angular size, peak column density, total flux, position angle, and degree of isolation, is presented. The data are characterized into several classes of anomalous-velocity H I emission. Most high-velocity emission features are HVCs and have a filamentary morphology and are loosely organized into large complexes extending over tens of degrees. In addition, 179 compact and isolated anomalous-velocity objects, CHVCs, are identified based on their size and degree of isolation. Of the CHVCs originally classified by Braun & Burton, 25% are reclassified based on the HIPASS data. The properties of all the high-velocity emission features and only the CHVCs are investigated, and distinct similarities and differences are found. Both populations have typical H I masses of $\sim 4.5 D_{\rm kpc}^2\, M_\odot$ and have similar slopes for their column density and flux distributions. On the other hand, the CHVCs appear to be clustered and the population can be broken up into three spatially distinct groups, while the entire population of clouds is more uniformly distributed with a significant percentage aligned with the Magellanic Stream. The median velocities are $V_{\rm GSR} = -38$ km s^{-1} for the CHVCs and -30 km s^{-1} for all the anomalous-velocity clouds. Based on the catalog sizes, high-velocity features cover 19% of the southern sky, and CHVCs cover 1%.

Key words: Galaxy: halo — intergalactic medium — ISM: H I — Local Group — Magellanic Clouds

On-line material: machine-readable tables

1. INTRODUCTION

Evidence for diffuse intergalactic material comes directly from intracluster X-ray emission at high redshift (Mulchaey 2000) and the Lyα absorber systems (Penton, Shull, & Stocke 2000). However, the amount of intergalactic neutral hydrogen at $z = 0$ remains highly uncertain, and its presence has important implications for the efficiency and timescales of galaxy formation and the epoch of reionization (Gnedin 2000; Rees 1986). If primordial concentrations of neutral gas exist, they could also house a large fraction of the missing mass in the universe (Moore et al. 1999; Klypin et al. 1999).

Anomalous-velocity concentrations of atomic hydrogen surround our Galaxy, and the formation and evolution of our Galaxy is evidently strongly linked to an environment that includes these objects, as well as the Galaxy's extended massive halo and the galaxies of the Local Group. These atomic hydrogen concentrations have velocities forbidden by simple models of Galactic rotation, and the debate continues over their distance and role in galaxy formation. Our ability to unravel their origin is complicated by the bulk classification of essentially all anomalous-velocity H I as a single type of object that does not conform with Galactic rotation and does not contain stars. In reality there are several classes of this anomalous emis-

[1] Research School of Astronomy and Astrophysics, ANU, Weston Creek P.O., Weston, ACT 2611, Australia.
[2] Australia Telescope National Facility, CSIRO, P.O. Box 76, Epping, NSW 2121, Australia.
[3] Currently a Hubble Fellow at the Center for Astrophysics and Space Astronomy, University of Colorado, Campus Box 389, Boulder, CO 80309; mputman@casa.colorado.edu.
[4] Sterrewacht Leiden, P.O. Box 9513, 2300 RA Leiden, Netherlands.
[5] Netherlands Foundation for Research in Astronomy, P.O. Box 2, 7990 AA Dwingeloo, Netherlands.
[6] Centre for Astrophysics and Supercomputing, Swinburne University, Mail No. 31, P.O. Box 218, Hawthorn, VIC 3122 Australia.
[7] Department of Physics and Astronomy, University of Wales, Cardiff, P.O. Box 913, Cardiff CF2 3YB, Wales.
[8] Department of Physics, University of Western Sydney Macarthur, P.O. Box 555, Campbelltown, NSW 2560, Australia.
[9] School of Physics, University of Melbourne, Parkville, VIC 3010, Australia.
[10] Department of Physics and Astronomy, University of New Mexico, 800 Yale Boulevard Northeast, Albuquerque, NM 87131.
[11] Jodrell Bank Observatory, University of Manchester, Lower Withington, Macclesfield, Chesire, SK11 6QS, England.
[12] Space Telescope Science Institute, 3700 San Martin Drive, Baltimore, MD, 21218.
[13] Anglo-Australian Observatory, P.O. Box 296, Epping, NSW 1710, Australia.
[14] School of Physics, University of Sydney, A28, Sydney, NSW 2006, Australia.
[15] Department of Physics and Astronomy, University of Leicester, University Road, Leicester LE1 7RH, England.

sion (e.g., see Wakker & van Woerden 1997; Putman & Gibson 1999), including high-velocity cloud complexes located within some 10 kpc of the Galactic plane, tidal streamers associated with the gravitational interaction of the Magellanic Clouds and the Milky Way, and compact, isolated clouds that may be scattered throughout the Local Group. The origins and physical relevance of anomalous-velocity H I emission can be more readily determined once a clear classification into subcategories has been made.

The possibility that some of the anomalous-velocity clouds are distributed throughout the Local Group has been considered earlier, by (among others) Oort (1966, 1970, 1981), Verschuur (1975), Eichler (1976), Einasto et al. (1976), Giovanelli (1981), Bajaja, Morras, & Pöppel (1987), Wakker & van Woerden (1997), Blitz et al. (1999), and Braun & Burton (1999). Blitz et al. (1999) showed that several general properties of the anomalous-velocity H I sky could be interpreted in terms of the hierarchical structure paradigm for the formation and evolution of galaxies. In this context, the extended, filamentary H I complexes, high-velocity clouds (HVCs), would be relatively nearby objects currently undergoing accretion onto the Galaxy or interacting with one of the Magellanic Clouds, while the compact, isolated objects, (CHVCs, following Braun & Burton 1999, hereafter BB99) would be their less evolved counterparts scattered throughout the Local Group environment, typically at distances of several hundred kiloparsecs and with H I masses of about 10^6 to 10^7 $M_\odot$.

BB99 stressed that the population of anomalous-velocity H I in the northern hemisphere can be split into distinct CHVC and HVC components when observed with the spatial sampling and sensitivity of the Leiden-Dwingeloo Survey of Hartmann & Burton (1997). The southern sky, however, has remained severely undersampled, leaving a major gap in our knowledge of the distribution of the compact clouds. Although HVC features are distributed over the entire sky (see Wakker & van Woerden 1997), most studies have focused on the northern complexes because of limited southern neutral hydrogen data. This paper characterizes the high-velocity H I sky south of decl. $+2^\circ$ and within the LSR (local standard of rest) velocity range -500 to $+500$ km s^{-1}, using data from the H I Parkes All-Sky Survey (HIPASS; Barnes et al. 2001), reduced with an algorithm that recovers extended emission (Putman et al. 2002; Putman 2000). The data allow the highest spatial resolution (15.5) large-scale study of the anomalous-velocity HVC and CHVC phenomena to date. Since these clouds show an increasingly complex structure at higher resolution (e.g., Wakker & Schwarz 1991; Braun & Burton 2000), HIPASS has great potential for providing new insights into these objects. The positional accuracy of HIPASS will also encourage further distance and metallicity determination work to be carried out in the southern hemisphere.

In this paper, we describe a catalog of the anomalous-velocity clouds detected by HIPASS that includes the distinction between compact and extended objects. The method of cataloging the clouds is described, and the spatial and kinematic distributions of high-velocity clouds and compact high-velocity clouds are discussed separately. The flux, column density, size, and position angle properties of the populations are also thoroughly investigated.

2. DATA AND CATALOG

2.1. *Observations*

The neutral hydrogen data are from the H I Parkes All-Sky Survey (HIPASS), reduced with the MINMED5 method (Putman et al. 2002; Putman 2000). HIPASS is a survey for H I in the southern sky, extending from the south celestial pole to declination $+2^\circ$, over velocities from -1280 to $+12700$ km s^{-1} (see Barnes et al. 2001 for a full description). The survey utilized the 64 m Parkes radio telescope, with a focal plane array of 13 beams arranged in a hexagonal grid, to scan the sky in 8° zones of declination with Nyquist sampling. The spectrometer has 1024 channels for each polarization and beam, with a velocity spacing of 13.2 km s^{-1} between channels and a spectral resolution, after Hanning smoothing, of 26.4 km s^{-1}. Each $8^\circ \times 1.^\circ7$ scan was reobserved five times (460 s beam^{-1} total integration time) to reach the full survey sensitivity. This repetitive procedure provides source confirmation, mitigates diurnal influences, and aids interference excision.

HIPASS was designed to detect discrete H I sources. In fact, the standard HIPASS reduction method described by Barnes et al. (2001) filters out emission that extends over more than 2° of declination. This is because a running median filter of this extent is used to provide a local bandpass calibration of each spectrum. Many of the anomalous-velocity H I objects are extended on larger angular scales, so an alternate method of bandpass calibration was developed (known as the MINMED5 method) that recovers emission that extends up to 7° in declination. MINMED5 calculates the bandpass correction for each beam, polarization, and velocity by first dividing the 8° scan into five sections, then finding the median emission in each section, and subsequently using the minimum of the five values. The MINMED5 procedure greatly increases the sensitivity of the data to large-scale structure without substantial loss of flux density, except when the emission fills the entire 8° scan. This circumstance occurs for H I emission from the Galactic plane and from the Magellanic Clouds. H I emission in the LSR velocity range -700 to $+1000$ km s^{-1} was reduced in this manner. Further details of the MINMED5 procedure are given by Putman et al. (2002) and Putman (2000).

The calibrated scans were gridded with the median method described by Barnes et al. (2001), without the weighting that overcorrects the fluxes for extended sources. The median method has the desirable effect of being robust to intermittent interference, but it causes the effective beam area, as well as the peak gridded response, to vary systematically with source size. Completely unresolved sources have a response reduced by a factor of 1.28, while sources larger than about $40'$ have the nominal response (as tabulated in Barnes et al.). We have taken account of this effect in our analysis. For unresolved sources the rms, determined from the data cubes using an iterative 3 σ clip, is 13 ± 1 mJy beam^{-1}. Although nominally the same as the Barnes et al. HIPASS sensitivity, it is slightly worse than expected, considering the greater velocity smoothing (26 km s^{-1}; cf. 18 km s^{-1}) in the current data. The difference appears due to the closer proximity in velocity to bright Galactic features. For extended sources, the rms noise is 10 mJy beam^{-1} (beam area 243 arcmin^2), corresponding to a brightness temperature sensitivity of 8 mK. The spatial size of the gridded cubes is $24^\circ \times 24^\circ$ with a few degrees of overlap between each cube.

2.2. *Cloud Search Algorithm and Selection Criteria*

The cataloged clouds were initially defined using data cubes that were smoothed spectrally by a Gaussian with FWHM 31 km s^{-1} and spatially with a Gaussian with FWHM 19′. The cloud parameters listed in the catalog (and in Table 1) were subsequently measured from the unsmoothed cubes (15.′5 spatial resolution and 26 km s^{-1} velocity resolution). The entire velocity range (-700 km s^{-1} $< V_{\rm LSR} <$ $+1000$ km s^{-1}) of the cubes was searched, excluding velocities $|V_{\rm LSR}| < 90$ km s^{-1}, where confusion with emission from the conventional Milky Way gaseous disk is difficult to avoid. The catalog includes only objects with velocities between ± 500 km s^{-1}, since no high-velocity cloud was found beyond this velocity range. The galaxies found beyond that range will be included in the HIPASS Bright Galaxy Catalog (Koribalski et al. 2002). All the detections within ± 500 km s^{-1} that correspond to known galaxies recorded in the LEDA and NED databases are included in the table and appropriately labeled but are excised from the figures. A total of 1997 anomalous-velocity H I objects are represented in the catalog, of which 41 are galaxies (one of which was previously unknown), 1618 are HVCs, 179 are CHVCs, and 159 are designated :HVC (see § 2.4). The median properties of the four categories of cataloged objects are listed in Table 2.

A full description of the cloud search algorithm is given by de Heij, Braun, & Burton (2002). The steps used to catalog the HIPASS clouds are briefly summarized as follows:

1. All pixels with $T_B > 6$ mK in the smoothed data cubes were examined, and each was assigned to a local maximum with which it is connected (spatially and in velocity; there are 26 neighboring pixels).
2. Only those local maxima with $T_B(\max) > 12$ mK were retained.
3. Adjacent local maxima were merged into a single cloud if the brightest enclosing contour for the particular maximum had $T_B > 80$ mK (i.e., if there exists a bright connection between the maxima) or if $T_B > 0.4T_B(\max)$ (i.e., if the contrast between the local maxima is small).
4. Finally, the merged maxima were labeled as clouds only if $T_B(\max) > 5\,\sigma$, where σ is the locally defined noise level at the velocity of each cloud candidate, determined from the clipped rms of pixel values within a $4^\circ \times 4^\circ$ box. Pixel values were clipped if they deviated by more than 3 times the absolute deviation from the median pixel value. The minimum noise value is 8 mK.

After following the above process to determine which pixels are part of a cloud, the unsmoothed data cubes were used to create integrated-intensity images that include the entire range of velocities of the pixels assigned to the cloud. Figure 1 shows two representative integrated-intensity maps of clouds cataloged in the above manner. A rectangular box defines the maximum spatial extent of the pixels assigned to each cataloged object in the figure. Because of the loss of the velocity information, the projected distribution shows the objects to overlap, but each pixel is assigned to only one object. Each integrated-intensity map and the spectrum in the direction of the object's peak brightness was also inspected by eye. A small number of obvious artifacts (e.g., due to failed bandpass calibration) were removed manually.

Finally, because the velocity cut of $|V_{\rm LSR}| < 90$ km s^{-1} does not exclude all emission directly associated with the Milky Way toward the Galactic plane (see Hartmann & Burton 1997), an additional selection criterion was applied to the catalog candidates, based on the deviation velocity, $V_{\rm dev}$. As defined by Wakker (1991), the deviation velocity of a cloud is the smallest difference between the velocity of the cloud and any allowed Galactic velocity in the same direction. The kinematic and spatial properties of the conventional Galactic H I were modeled to determine the deviation velocity from the local standard of rest velocity. The model (see de Heij et al. 2002) consists of a thin disk that has constant properties (volume density, scale height, and temperature) within the solar radius but flares and warps farther outward. The gas exhibits circular rotation with a flat rotation curve of 220 km s^{-1}. The velocity is considered an acceptable Galactic velocity as long as the intensity of the synthetic H I spectra at that position exceeds 0.5 K. We required that $|V_{\rm dev}|$ be greater than 60 km s^{-1} for the feature to be included in the catalog. Based on these criteria, some 209 candidates, or approximately 10%, were excluded from the catalog. The excluded objects probably include some whose appearance is due to small-scale structure in the gaseous disk of the Milky Way, but they may also include bona fide HVCs, CHVCs, or external galaxies. Several HVC populations included in the Wakker & van Woerden (1991, hereafter WvW91) catalog have $|V_{\rm dev}| < 60$ km s^{-1} and are thus excluded from this catalog (e.g., Populations Corotating, OA, and GCP). Those objects that have emission at high velocities, $|V_{\rm dev}| > 60$ km s^{-1}, but that clearly link to gas with $|V_{\rm dev}| < 60$ km s^{-1} are cataloged separately and referred to as XHVCs (see Table 3). There are 186 XHVCs and four galaxies that merge with low-velocity Galactic

TABLE 1

HIPASS Catalog of Anomalous-Velocity Objects (-500 km s^{-1} $< V_{\rm LSR} <$ 500 km s^{-1}; Decl. $< +2^\circ$)

No. (1)	Designation (ll ± bb ± vvv) (2)	R.A. (J2000.0) (3)	Decl. (J2000.0) (4)	$v_{\rm LSR}$ (km s^{-1}) (5)	$v_{\rm GSR}$ (km s^{-1}) (6)	$v_{\rm LGSR}$ (km s^{-1}) (7)	FWHM (km s^{-1}) (8)	Maj (deg) (9)	Min (deg) (10)	P.A. (deg) (11)	Size (deg^2) (12)	$T_{\rm peak}$ (K) (13)	$N_{\rm H\,I}$ (10^{20} cm^{-2}) (14)	Flux (Jy km s^{-1}) (15)	Galaxy (16)
1.....	HVC 000.0−59.4−114	22 36.5	−39 42	−114	−114	−115	40	0.3	0.2	40	0.11	0.05	0.04	5.9	...
2.....	HVC 000 .2−11.5−233	18 33.7	−34 13	−233	−232	−286	36	0.1	0.1	60	0.12	0.11	0.07	7.0	...
3.....	HVC 000.4−82.5+109	00 21.9	−30 58	109	110	136	38	0.3	0.2	20	1.19	0.15	0.12	91.2	...
4.....	HVC 000.4+06.7+122	17 21.1	−24 59	122	124	58	46	0.2	0.2	−40	0.14	0.09	0.07	5.8	...
5.....	HVC 000.5−75.8+173	23 53.4	−34 01	173	174	192	50	0.2	0.2	−40	0.44	0.16	0.16	32.3	...

Note.—Table 1 is presented in its entirety in the electronic edition of the Astronomical Journal. A portion is shown here for guidance regarding its form and content. Units of right ascension are hours and minutes, and units of declination are degrees and arcminutes. See also http://wwwatnf.atnf.csiro.au/research/multibeam.

TABLE 2
MEDIAN PROPERTIES OF CATALOGED OBJECTS (Decl. $< 2°$; -500 km s^{-1} $< V_{LSR} <$ $+500$ km s^{-1})

Class	N	V_{LSR} (km s^{-1})	V_{GSR} (km s^{-1})	V_{LGSR} (km s^{-1})	FWHM (km s^{-1})	$N_{H\,I}$ (10^{20} cm^{-2})	T_{peak} (K)	Flux (Jy km s^{-1})	Size (deg^2)	Maj (deg)	Min (deg)
HVCs.....	1618	117	−30	−62	36	0.08	0.12	19.0	0.42	0.3	0.2
CHVCs.....	179	95	−38	−57	35	0.14	0.2	19.9	0.36	0.2	0.2
:HVCs.....	159	105	−22	−66	36	0.12	0.16	17.0	0.35	0.2	0.2
All clouds.....	1956	114	−30	−63	36	0.09	0.12	19.0	0.41	0.3	0.2
GLXYs.....	41	386	264	218	57	0.33	0.34	55.5	0.28	0.2	0.1

emission galaxies are included in the XHVC catalog. The NGC 253, 292 [the Small Magellanic Cloud], and 301, and IC 5152.

2.3. *Catalog*

The results of the MINMED5-reduced HIPASS data and the anomalous-velocity cloud finder described above are given in the catalog, which begins in Table 1. As discussed in § 2.1, sources less than 40′ in diameter have had their brightness corrected for based on the object's angular size, by using the values listed in Table 3 of Barnes et al. The catalog contains the following entries: Column (1) lists the HIPASS HVC running number. Column (2) lists the designation, consisting of a prefix followed by the Galactic longitude, Galactic latitude, and local standard of rest velocity. The prefix is HVC for filamentary features and their substructures, which are organized into large high-velocity cloud complexes, CHVC for those satisfying the criteria of compact, isolated, high-velocity clouds (as discussed in § 2.4), :HVC for clouds that could not be unambiguously classified as CHVCs, and GLXY for galaxies cataloged in either the LEDA or the NED databases or visible in Digital Sky Survey (DSS) data. The DSS data were retrieved from the Space Telescope Science Institute for a 30′ diameter field centered on each catalog entry with velocity in excess of 100 km s^{-1}. Integer-rounded positions are used for larger sources, while an extra decimal place is used for the smaller ones. The Galactic longitude and latitude were calculated from the intensity–weighted average of the right ascension and declination (cols. [3]–[4]). Columns (3) and (4) list the intensity-weighted average (J2000.0) right ascension and declination of all pixels that are part of the object. Column (5) lists the intensity-weighted average local standard of rest velocity of all pixels in the object. Columns (6) and (7) list the average velocities, expressed in the galactic standard of rest and in the Local Group standard of rest frames. The galactic standard of rest reference system is defined by $V_{GSR} = 220 \cos b \sin l + V_{LSR}$; the Local Group standard of rest system, by $V_{LGSR} = V_{GSR} - 62 \cos l \cos b + 40 \sin l \cos b - 35 \sin b$, following BB99. Column (8) lists the velocity FWHM from the spectrum that passes through the peak T_B pixel of the object. Those values below 26 km s^{-1} (the velocity resolution) should be thought of as having 26 km s^{-1} as the upper limit. Columns (9), (10) and (11) list the angular semimajor axis, semiminor axis, and position angle of the full width at half-power (FWHP) ellipse in degrees. Using the velocity-integrated column density image of the object, an ellipse was fitted to the contour with half the value of the maximum column density (col. [14]). Thus the major and minor axes are not defined by the original pixels assigned to the object, as the other parameters are, but from the column density image. In almost all cases, the area from the major and minor axes is smaller than the area from the total number of pixels assigned to the cloud, but in a few cases it is larger because of the column density image includ-

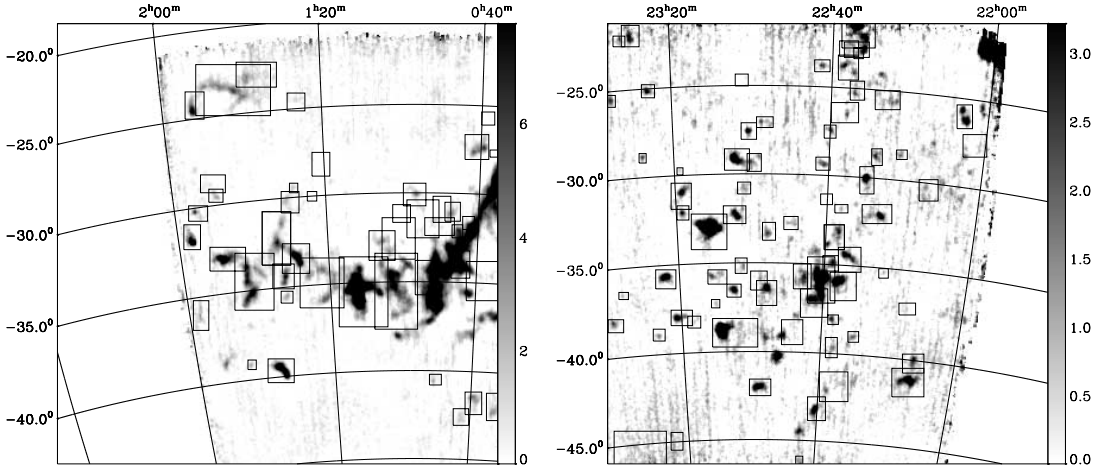

FIG. 1.—Representative column density images of two areas of the sky. *Left*, H I emission centered on the cloud HVC 245.3−79.5−096, integrated over the velocity range from -73 to -152 km s^{-1}; *right*, HVC 012.4−60.5−136, integrated from -86 to -152 km s^{-1}. The gray-scale bar indicates the intensity scaling in K km s^{-1}. Each cloud is indicated by a box that encloses all pixels identified with the cloud. All the clouds cataloged from these two areas of the sky and found to have some emission within the velocity ranges are indicated by boxes, including those centered at velocities outside the integration ranges represented in these two panels. Those boxes that appear empty indicate clouds that have only their velocity extremes within the image. The more extended clouds in the left-hand image are not cataloged because they merge with emission at the conventional velocities associated with the Milky Way.

TABLE 3

XHVCs, Objects with High-Velocity Emission (-60 km s$^{-1} > V_{DEV} > 60$ km s^{-1}) that Merge with Galactic Emission below This Velocity Range

No.	Designation (ll ± bb ± vvv)	R.A. (J2000.0)	Decl. (J2000.0)	v_{LSR} (km s^{-1})	v_{GSR} (km s^{-1})	v_{LGSR} (km s^{-1})	FWHM (km s^{-1})	Maj (deg)	Min (deg)	P.A. (deg)	Size (deg)^2	T_{peak} (K)	$N_{H\,I}$ (10^{20} cm^{-2})	Flux (Jy km s^{-1})	Galaxy
1.....	XHVC 000.2+07.0−095	17 19.6	−25 01	−95	−94	−160	39	0.6	0.4	83	6.49	1.73	1.23	1506.2	...
2.....	XHVC 001.3+05.0−089	17 29.8	−25 13	−89	−85	−148	34	0.5	0.3	56	1.68	1.19	0.73	365.0	...
3.....	XHVC 002.7−03.1+132	18 04.0	−28 11	132	143	85	40	0.2	0.2	−37	0.81	0.72	0.57	122.1	...
4.....	XHVC 004+05−095	17 35.2	−23 17	−95	−81	−143	29	12.1	8.3	−48	1.28	0.68	0.33	124.3	...
5.....	XHVC 004.3+05.1−097	17 36.6	−22 34	−97	−81	−142	36	0.6	0.3	−44	2.66	1.14	0.98	555.7	...

Note.—Table 3 is presented in its entirety in the electronic edition of the Astronomical Journal. A portion is shown here for guidance regarding its form and content. The complete XHVC table includes four galaxies. See also http://www.atnf.atnf.csiro.au/research/multibeam.

ing overlapping features. These size values were predominantly used to determine the designation. The position angle is positive in the direction of increasing Galactic longitude, with a value of zero when the object is aligned pointing toward the Galactic north pole. Column (12) lists the angular size based on the total number of pixels assigned to an object times the area of a $4' \times 4'$ pixel. Column (13) lists the peak brightness temperature in kelvins. Column (14) lists the maximum column density in 10^{20} cm^{-2}. Column (15) lists the total flux in jansky-kilometers per second. Column (16) lists the name of any previously cataloged galaxy in the LEDA or NED databases. Newly discovered galaxies (based on the fact that they are not in LEDA or NED) that have an optical counterpart in the DSS data have been given a HIPASS J2000.0 name designation. If the object has a clearly discernable optical counterpart it is followed by "(A)," if it does not, and has a GSR velocity exceeding 300 km s^{-1}, it is followed by "(B)."

Among the objects cataloged there will be a substantial number that are not new discoveries. We have not made cross-references to earlier detections, except for those objects identified with nearby galaxies named in the LEDA or NED compilations. Firmly establishing cross-references to earlier work would be a difficult matter, as in almost all cases the angular resolution and sensitivity of the HIPASS data are superior to earlier data. Earlier work established the general outlines of the major complexes, including the Magellanic Stream. Many of the HIPASS cataloged entries fall within these general outlines but are seen as separately indentifiable substructures at the HIPASS resolution. Examples of just a few of the cataloged objects that have been subject to substantial earlier work are given below:

HIPASS HVC No. 91, HVC 008.2−04.6−214, and HIPASS HVC No. 93, HVC 008.4−04.4−213, were discovered by W. Shane in Dwingeloo observations and reported by Oort (1968) and Hulsbosch (1968) before being subject to a more extensive analysis based on new data by Saraber & Shane (1974; see also Mirabel & Franco 1976). Shane's object is identified as two objects in the higher resolution HIPASS material. It is listed by WvW91 as their No. 307.

HIPASS HVC No. 605, CHVC 217.7 + 00.1 + 278, has been discussed as Dw 217.8 + 0.0 by Henning (2000) and Rivers (2000) as a nearby galaxy hidden behind the zone of avoidance and discovered in the Dwingeloo Obscured Galaxies Survey (see Henning et al. 1998). It is also listed by Henning et al. (2002) as HIZSS 003, at $l = 217\overset{\circ}{.}7$, $b = +0\overset{\circ}{.}08$. As no optical identification has yet been made, we retain the object as a CHVC, though it could be one of many nearby galaxies masquerading as a CHVC.

HIPASS HVC No. 1914, HVC 346.5 + 35.6−107, was the subject of Westerbork synthesis imaging carried out by Stoppelenburg, Schwarz, & van Woerden (1998). Stoppelenburg et al. cross-reference object 132 in the tabulation of WvW91, although that object is located some 2° distant from the HIPASS position, illustrating the difficulties with detailed cross-referencing between catalogs with such different observational parameters. Besides the resolution difference for the southern part of the WvW91 catalog (35′ beam on a $2^\circ \times 2^\circ$ grid), they also merged clouds by examining the individual components by eye for a spatial connection at similar velocities.

2.4. *Definition of a Compact, Isolated High-Velocity Cloud*

The early surveys for high-velocity clouds were based on rather coarse sampling of the sky and only modest sensitivity, and this made it difficult to assess the cloud's morphology or to make more than the simplest organization of objects into "complexes." With the advent of more finely sampled sensitive surveys it has become possible to utilize source morphology in the process of classification. BB99 investigated the Leiden-Dwingeloo Survey (LDS) of Hartmann & Burton (1997) and found a dichotomy in the types of H I emission features seen at anomalous velocity. The large majority of high-velocity emission originates in relatively diffuse filaments that are organized into complexes extending over large regions of the sky. There is substructure in these filaments, but it is generally consistent with only modest changes in the viewing geometry and the line-of-sight overlap of a population of intrinsically elongated structures extending over many degrees on the sky. In addition, they recognized a second type of high-velocity cloud, namely, compact, isolated objects with a high column density contrast. The H I signatures of these objects are indistinguishable from those of many dwarf galaxies. As stated in the introduction, BB99 refer to this subclass of compact, isolated clouds as CHVCs and argue that the kinematic and spatial properties of the CHVCs suggest Local Group distances and a net infall velocity of about 100 km s^{-1} toward the barycenter of the Local Group. Since the sample of BB99 was drawn from the Leiden-Dwingeloo Survey (by eye), their study did not include clouds south of decl. -30° nor more detail than that afforded by the 35′ resolution of the data.

The spatial resolution and sky coverage of the MINMED5 processed HIPASS make it an ideal data set for the study of CHVCs in the southern sky. The combination of high-resolution, Nyquist-sampled imaging, and high sensitivity reveal distinct morphological features associated with the different categories of high-velocity H I. The Magellanic Stream, for example, is characterized by extremely long filaments (typically $>10^\circ$ in extent) with a preferred

alignment (parallel to the great circle formed by R.A. = 23^h and 11^h), while the extended accumulations at positive LSR velocities in the third longitude quadrant first observed by Wannier & Wrixon (1972) and Wannier, Wrixon, & Wilson (1972) have a completely different "texture," consisting of shorter filaments (typically 5° to 10°) with a wide range of orientations. The CHVCs stand out from this filamentary background, more so than with the coarser resolution of the LDS. It seems likely that the distinctive resolved morphologies of different anomalous-velocity objects might be used to better classify those objects that share a common physical origin. Here only the basic distinction between the filamentary HVC complexes and the CHVCs is examined.

The selection criteria for a CHVC was applied to a $10^\circ \times 10^\circ$ velocity-integrated intensity image centered on each object, including all pixels with a brightness greater than 6 mK. The overriding consideration for the CHVC classification was the brightness distribution at a level corresponding to about 25% of the peak column density of each object. It was required that this contour (1) be closed with an angular size less than 2°, (2) not be elongated in the direction of any lower level extended emission, and (3) be more than 3 σ above the local noise floor, so that the assessment of elongation is meaningful. In this way we hoped to avoid the low-contrast local maxima found along filamentary features, as well as local maxima formed by the line-of-sight overlap of several filaments. Sources clearly satisfying all three requirements were designated CHVC in the catalog. Those sources that satisfied the size and signal-to-noise requirements but could not be unambiguously classified with regard to their elongation were designated :HVC, while all remaining sources were given the HVC designation. Although the first and last of these conditions are straightforward to apply, the second is difficult to incorporate into a digital algorithm and was therefore applied interactively. Since some subjectivity is involved in this assessment, two of the authors (V. d. H. and R. B.) independently carried out a complete classification of all sources. Identical classification was given to 98.9% of the sample, suggesting that the criterion can be applied repeatably. A consensus on classification was reached on the remaining 25 sources after reexamination. Figure 2 shows an example of typical objects classified as CHVCs, :HVCs, and HVCs.

2.5. *Completeness of the Catalog*

Each cloud is automatically confirmed in the HIPASS data because of the repetitive nature of the survey and the overlap between adjacent scans (see Barnes et al. 2001). Therefore reobservation and confirmation of each object, such as done by BB99, is not required. A recent analysis of the Arecibo Dual Beam Survey (Schneider & Rosenberg 2000) has shown that full survey completeness for compact sources is reached only at significance levels exceeding about 8 σ. In the case of the CHVCs, we have required, as noted above, that the contour at 25% of peak brightness must be above 3 σ in the velocity-integrated image, so that the peak column density must exceed 12 σ. Since the typical CHVC FWHM line widths are only marginally resolved at 26 km s^{-1}, this corresponds to a limiting peak column density of about 6×10^{18} cm^{-2} for CHVC detection. The corresponding flux density limits for unresolved sources are $\sim$2 Jy km s^{-1} for HVCs and $\sim$4 Jy km s^{-1} for CHVCs. For mainly unresolved galaxies of low velocity width in the south celestial cap region, Kilborn, Webster, & Staveley-Smith (1999) quote a similar HIPASS completeness limit of 4 Jy km s^{-1}.

The nature of the cloud-cataloging algorithm, however, leads to surprisingly poorer completeness and reliability levels than those expected from the above discussion. Although many low flux density galaxies are represented in the catalog, comparison with the literature shows a systematic tendency to underestimate the total flux density for objects with measured values as high as $\sim$25 Jy km s^{-1}. Completeness and reliability for extended clouds are also poorer, as these objects cover many pixels. Typically, truncation of the low column density wings occurs, leading to an underestimate of total flux density. Our present understanding of the completeness limits are that the catalog is complete above $\sim$25 Jy km s^{-1} in flux density and $\sim 10^{19}$ cm^{-2} in column density.

The above discussion has assumed a uniform noise level and a sufficiently low source density that confusion does not become a problem for source recognition and detection. While this is appropriate for a large fraction of the position-velocity volume of the data, there are also large regions that are adversely affected both by an increased noise level and source confusion. The most prominent of these is the gap between $V_{dev} = -60$ and $+60$ km s^{-1}, which we leave

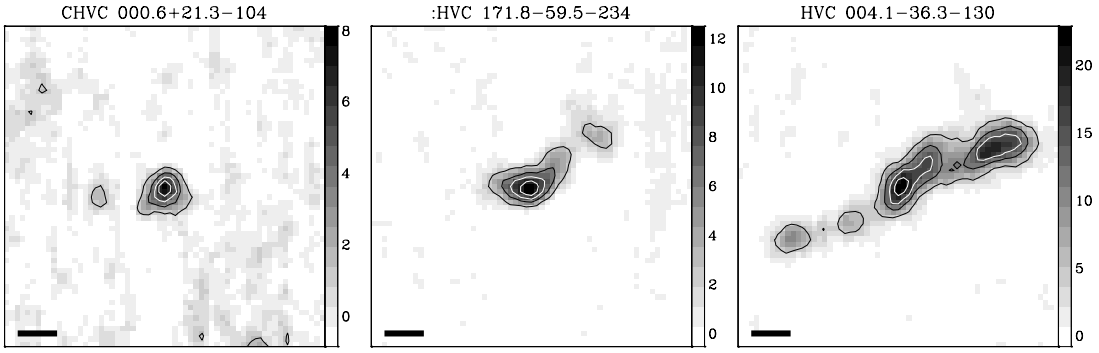

FIG. 2.—Cloud classification. The integrated H I emission over the velocity extent of each of the three objects is shown in a $10^\circ \times 10^\circ$ field. The gray-scale wedge indicates the intensity scaling in K km s^{-1}. Contours are drawn at 30, 50, 70, and 90% of the peak column density. The heavy bar at lower left indicates a length of 2°. *Left*, object given the CHVC designation, based on the absence of elongation of the 30% contour along filamentary structure in the field; *middle*, object given the :HVC designation, since there is some ambiguity in its elongation; *right*, object classified as HVC, based on the clear extension of the 30% contour.

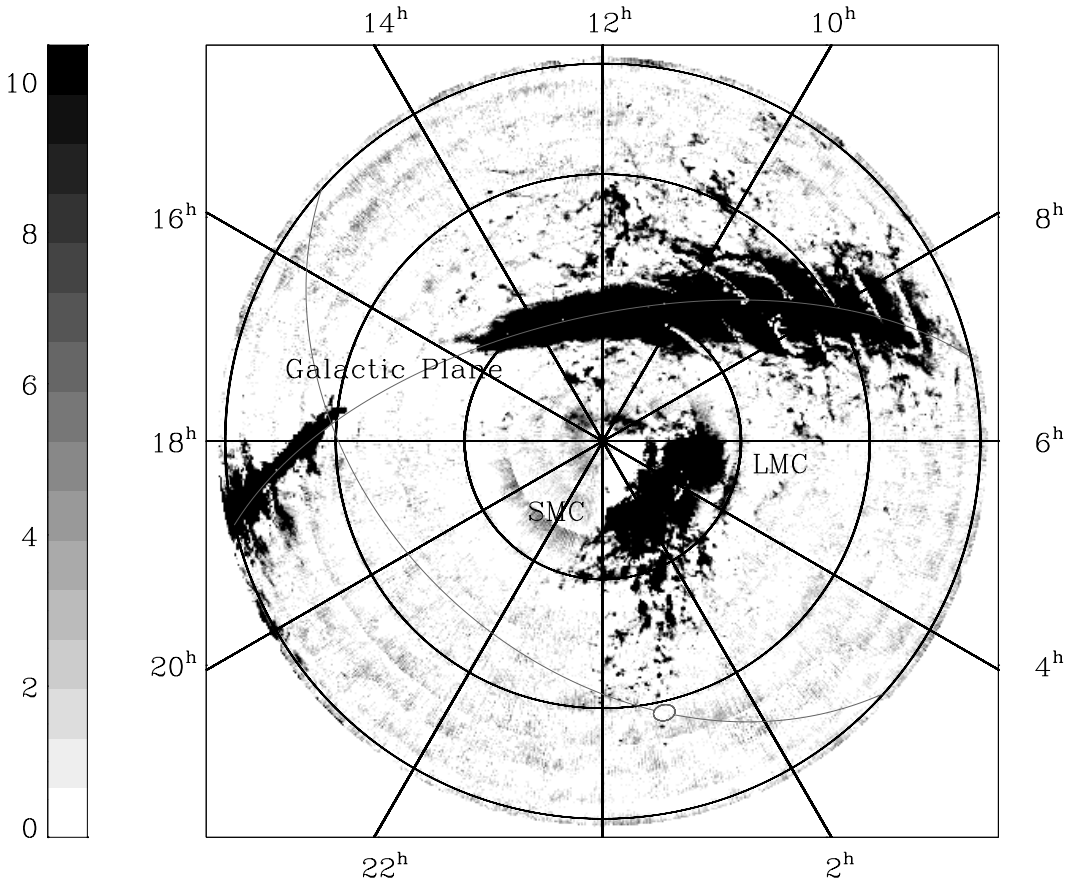

FIG. 3.—Integrated-intensity map of the anomalous-velocity HIPASS sky in a south celestial pole projection showing emission at positive velocities ranging from $V_{LSR} = 99$ to 500 km s^{-1}. The declination circles are in increments of 30°. The Galactic equator and the great circle at $l = 0°$ are indicated with solid lines, while the south Galactic pole is indicated with an open circle. The gray-scale bar on the left indicates the intensity scale in K km s^{-1}. The Large and Small Magellanic Clouds (LMC and SMC) and the Galactic plane dominate the intensities in this velocity range, and much of their emission is saturated in this gray-scale image. The Magellanic Bridge (between the LMC and SMC), the portion of the Magellanic Stream in this velocity range (between the Clouds and the south Galactic pole), and the Leading Arm (between the Clouds and the Galactic plane) are also shown. The Galactic plane shows some effect of the emission filling the entire 8° scan and being affected by the bandpass correction (see Putman et al. 2002).

entirely out of consideration because of confusion with Galactic emission. In addition, the data volumes occupied by the Large and Small Magellanic Clouds, the Magellanic Stream, and the major HVC complexes, give rise to an effective increase in the rms fluctuation level and a reduced ability to detect potentially unrelated anomalous-velocity objects that overlap in the measurement volume. Therefore, we note that the catalog may not be complete to the stated levels in these regions.

This catalog will be combined with a new catalog of the northern sky to obtain a complete all-sky CHVC catalog (de Heij et al. 2002). However, the issue of the superior spatial resolution, but inferior velocity resolution, of the HIPASS material compared with that of earlier surveys does not make the combination immediately straightforward. To obtain a uniform catalog with similar sensitivities and velocity information, it may be required to spatially smooth the HIPASS data and kinematically smooth the northern sky data.

There are 30 of the 65 CHVCs in the BB99 catalog that are found between decl. −30° and +02° and are therefore also cataloged here. In general, the position, velocity, FWHM, peak brightness temperature, and column density properties of the clouds in both catalogs agree. The largest difference is the degree of isolation, or the designation as CHVC, :HVC, or HVC, with 50% of the BB99 CHVCs in the region of overlap reclassified as HVCs or :HVCs. The central velocities of the two catalogs agree within 10 km s^{-1}, and the FWHMs closely match when the LDS is smoothed to HIPASS velocity resolution. The average difference in the size of the major axis is 20′; however, the size is based on the 50% T_{max} contour in BB99 (all the resolution allowed for) and the 25% T_{max} contour here. T_{max} agrees within 32% and $N_{H\ I}$ within 45%, with the HIPASS value generally higher in both cases. These results make sense when one considers the different resolutions of the surveys. The improved spatial resolution of HIPASS changes the size of the cloud, and its decrease in velocity resolution and increased sensitivity may both be partially responsible for the change in isolation criteria. The variation in column density for HVC sight lines at different resolutions is expected, and this effect has been fully discussed by Wakker, Oosterloo, & Putman (2002) and Wakker et al. (2001).

The positional accuracy was tested by comparing the published positions of the galaxies in the catalog with the HIPASS values. The positions generally agree within 2′ and almost always within 10′.

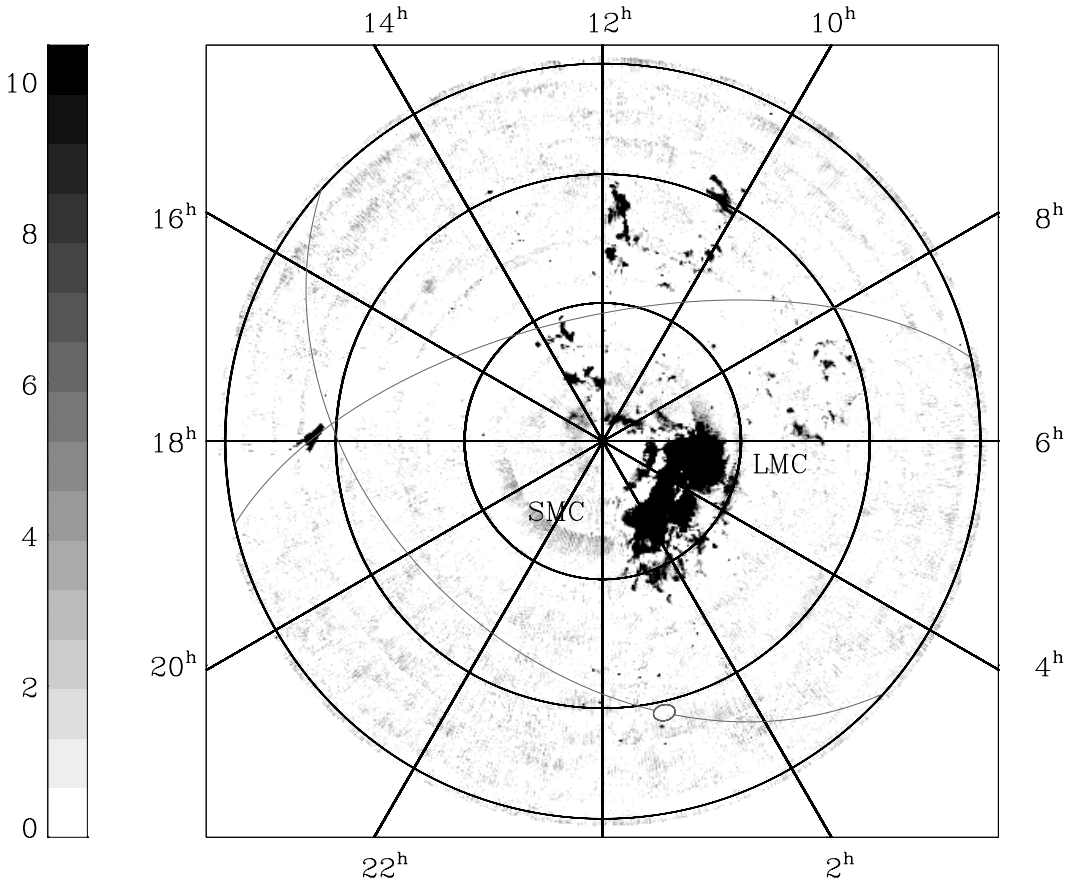

FIG. 4.—Integrated-intensity map of the anomalous-velocity HIPASS sky at more extreme positive velocities than those in Fig. 3. This map includes $V_{LSR} = 200$ to 500 km s^{-1}, a range that excludes most of the emission from the Galactic plane. The LMC, the Magellanic Bridge, and the Leading Arm dominate the H I flux observed, but numerous other HVC and CHVC features are evident.

3. RESULTS

3.1. *General Distribution Properties*

Column density images of the high-velocity H I sky are shown in polar cap projection for three representative ranges of anomalous velocities in Figures 3, 4, and 5. The Magellanic Clouds, portions of the Magellanic Stream, and the Milky Way gaseous disk dominate the perceived fluxes and are labeled in the figures. The emission from the Galactic plane is not cataloged, but the LMC and several low-velocity galaxies are cataloged and identified. The SMC merges with low-velocity Galactic emission (gas with $V_{dev} < 60$ km s^{-1}) and is included only in the catalog of XHVCs (Table 3). Several properties of the high-velocity gas are evident in Figures 3–5, including the broad range of spatial structures of the high-velocity features, the difficulty in defining an HVC based on the LSR definition near the Galactic plane, and the clear dichotomy in the location of the positive and negative LSR velocity features (negative predominantly at $l < 180°$ and positive at $l > 180°$).

The spatial distribution of all the cataloged HIPASS anomalous-velocity objects is shown in the same polar cap projection in Figure 6, with the objects' GSR velocity represented. No distinction is made in this plot between objects identified in the catalog as HVCs, :HVCs, or CHVCs, and the GLXYs are not included. The figure shows local minima in the density of objects along the Galactic disk and toward the Magellanic Clouds, where the survey completeness is expected to degrade (as discussed in § 2.5). The band of objects extending from near $(\alpha, \delta) = (0^h, 0°)$ to $(4^h, -50°)$ contains the Magellanic Stream and the highest negative GSR velocities. The large positive velocity accumulation (designated WA, WB, WC, and WD by WvW91) first noted by Wannier & Wrixon (1972) and Wannier et al. (1972) is concentrated between $(\alpha, \delta) = (9^h \rightarrow 12^h, -10° \rightarrow -50°)$. This region also contains material that is most likely related to the Magellanic Leading Arm (Putman et al. 1998), as shown in Figure 4. Other known complexes evident in this figure include complex L, centered near $(\alpha, \delta) = (15^h, -30°)$, parts of the GCN and GCP complexes, near $(\alpha, \delta) = (21^h, -10°)$, and the tail of complex C, near $(\alpha, \delta) = (17^h, -10°)$. The GCN and GCP complexes appear to be part of an extension of clouds that extend through the south Galactic pole, perpendicular to the Magellanic Stream. A striking feature of the distribution is the paucity of anomalous-velocity H I in the region bounded approximately by $(\alpha, \delta) = (2^h \rightarrow 5^h, -10° \rightarrow -30°)$.

The perceived structure of many of the concentrations of anomalous-velocity H I emission is dependent on the projection used. The distribution of the 1956 cataloged clouds in Galactic coordinates is shown in Figure 7, with the spatial limits of the catalog represented by the dotted line. The distribution of clouds is similar to that presented by WvW91 (and also to the distribution of high-velocity components presented by Morras et al. 2000), but there is a factor of ~4 increase in the number of individual clouds south

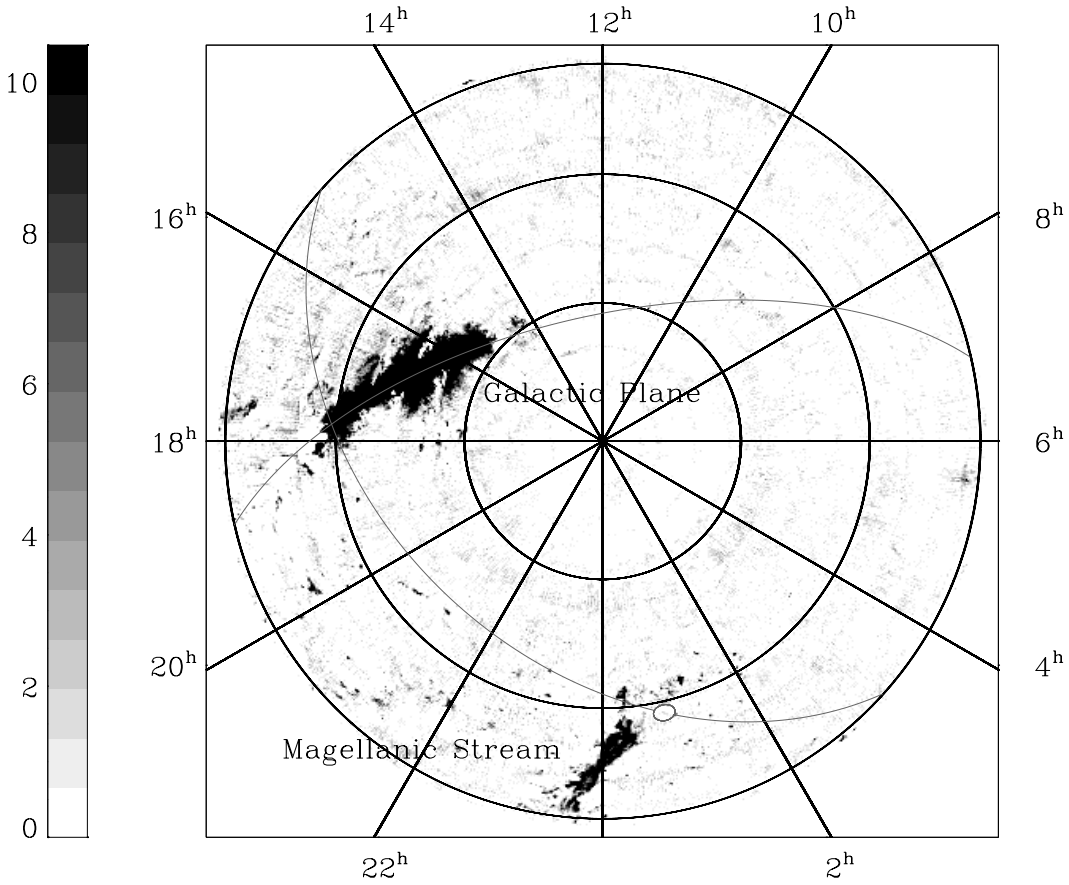

FIG. 5.—Integrated-intensity map of the anomalous-velocity HIPASS sky at negative velocities extending from $V_{LSR} = -99$ to -500 km s^{-1} in the same projection as Fig. 3. Portions of the Magellanic Stream and of the Galactic plane dominate the emission at these velocities and are indicated.

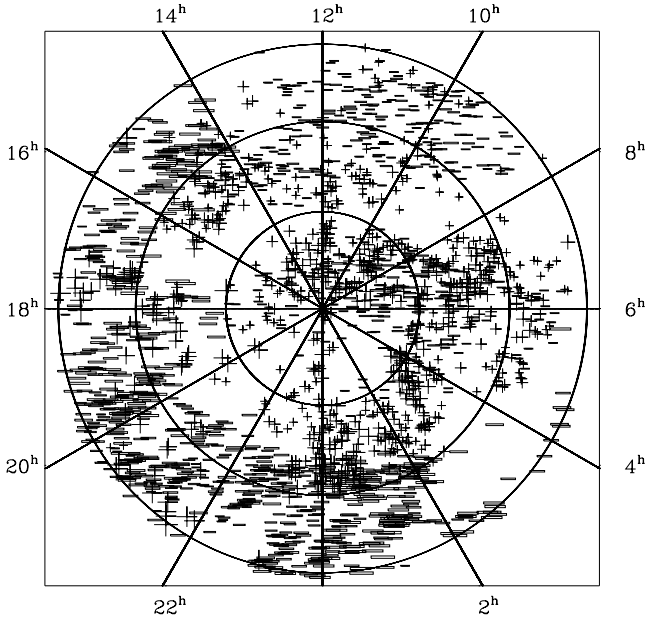

FIG. 6.—Distribution of all anomalous-velocity objects cataloged (HVCs, CHVCs, and :HVCs) in the south polar cap projection. The declination circles are in increments of 30°. No distinction is made here between the extended HVCs and the compact CHVCs. Plus and minus signs are used to indicate positive and negative velocities in the GSR frame, with the size of the sign proportional to magnitude of their GSR velocity.

of decl. 2° compared with that in the WvW91 catalog. This increase in the number of individual clouds is due to both the improvement in spatial resolution and the catalog method.

The kinematic distribution of all the cataloged anomalous-velocity objects (i.e., HVCs, :HVCs, and CHVCs) is plotted against Galactic longitude and latitude in Figures 8 and 9, respectively, for the Local, Galactic, and Local Group reference frames. As noted previously, the majority of the southern anomalous-velocity objects at $l > 180°$ are at positive LSR velocities, and though the number of objects

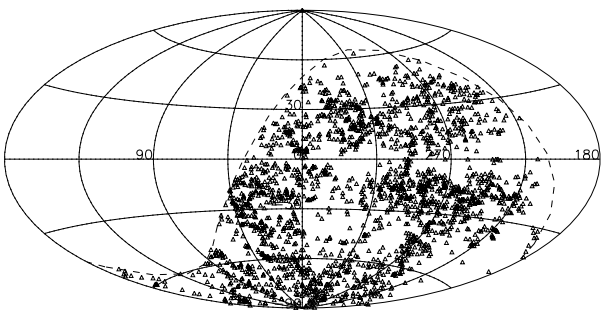

FIG. 7.—Distribution of all anomalous-velocity objects cataloged in Galactic coordinates: $l = 0°$ is in the center of this figure and increases in increments of 45° to the left; b increases in increments of 30°.

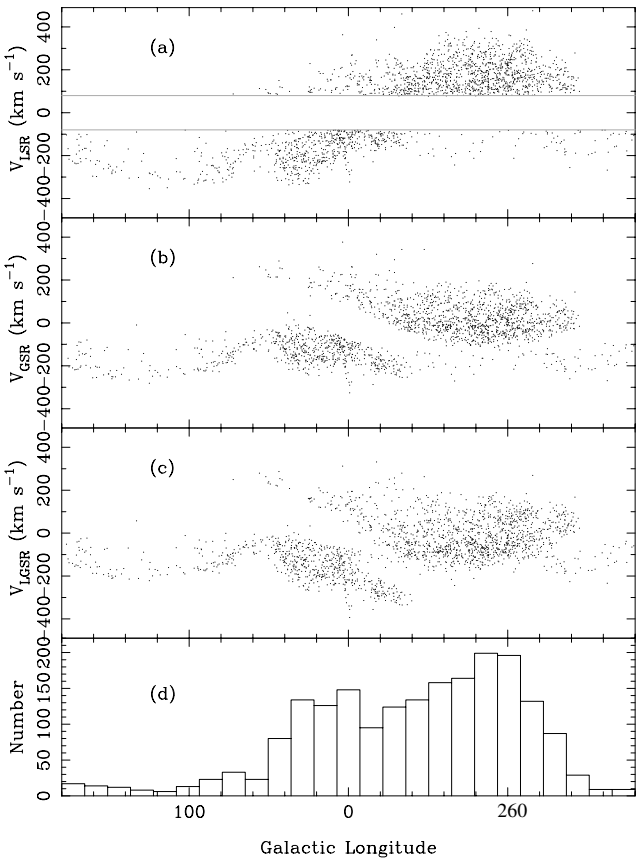

FIG. 8.—Velocities of all the anomalous-velocity objects identified in the HIPASS data, plotted against Galactic longitude for three different kinematic reference frames: (*a*) with respect to the local standard of rest; (*b*) with respect to the Galactic standard of rest; (*c*) with respect to the Local Group standard of rest. (*d*) Number of high-velocity clouds in terms of Galactic longitude.

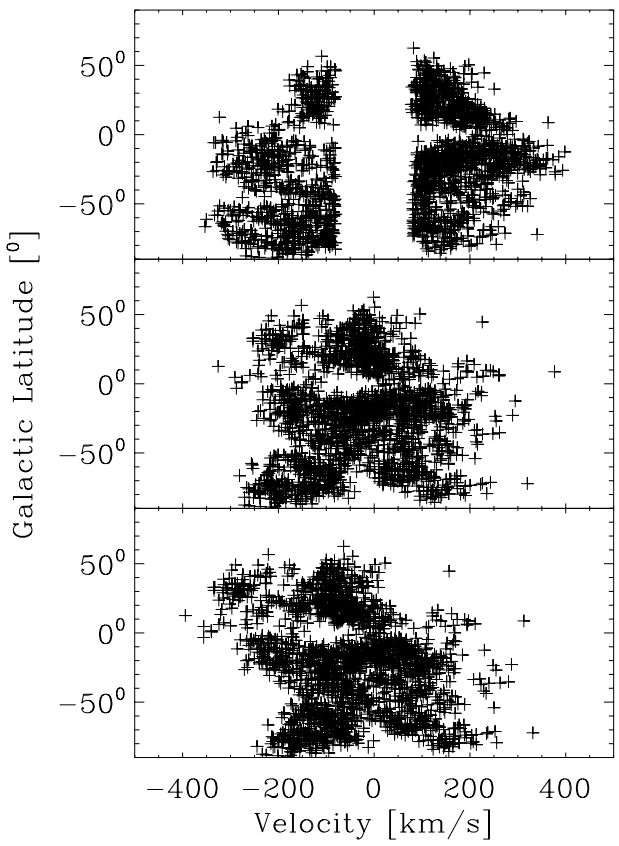

FIG. 9.—Galactic latitude vs. velocity for all the anomalous-velocity objects identified in the HIPASS data, in three different kinematic reference frames: *top*, with respect to the local standard of rest; *middle*, with respect to the Galactic standard of rest; *bottom*, with respect to the Local Group standard of rest.

at $l < 180^\circ$ is small, they are predominantly at negative LSR velocities. This follows the trend of the rotating Galactic H I (Burton 1988), but of course the magnitude is much greater. The largest range of velocities in every reference frame is at $l = 0^\circ$. In fact, some of these clouds become more positive or negative in the GSR frame. The distribution of the clouds in the Local Group reference frame (Fig. 8*c*) is not greatly different from the Galactic reference frame; the clouds are slightly more spread out and the broad distribution at $l = 0^\circ$ remains. The number of clouds at each Galactic longitude is presented in Figure 8*d*, but note it is not complete at all longitudes, as shown in Figure 7. The overabundance of clouds around $l \approx 270^\circ$ is primarily due to the Magellanic Stream, which is a prominent feature in Figures 8 and 9. In Figure 9 the Stream provides a large component of the negative-latitude gas, particularly the concentration near (V_{GSR}, b) = (-200 km s^{-1}, -70°). The Magellanic Leading Arm (Putman et al. 1998) is represented by the clouds near the Galactic plane that remain at high velocities.

Histograms of the various velocity distributions are shown in Figure 10. The formal standard deviations of the distributions are 115 km s^{-1} in both the GSR and the LGSR systems, compared with 185 km s^{-1} in the LSR frame. Blitz et al. (1999) found a similar decrease between the LSR and GSR dispersions using the all-sky WvW91 catalog and excluding the Magellanic Stream. Because of the large gap in survey coverage at low LSR velocities, the LSR value is an upper limit. The median LSR velocity for the HIPASS catalog is 114 km s^{-1}, while the median in the GSR distribution is at approximately -30 and -63 km s^{-1} in the LGSR system. Of course, the high-velocity objects of the northern hemisphere, where negative velocities dominate, should also be included in this analysis before conclusions are drawn on the clouds' overall distribution. The all-sky WvW91 catalog has median velocities of -90 (LSR), -38 (GSR), and -58 km s^{-1} (LGSR). Mean velocities are -33 (LSR), -48 (GSR), and -46 km s^{-1} (LGSR) for the all-sky WvW91 catalog, and 44 (LSR), -33 (GSR), and -54 km s^{-1} (LGSR) for the southern HIPASS catalog.

The distributions of several properties of the cataloged objects are shown in Figures 11 to 14, and the median properties are tabulated in Table 2. The distribution functions of H I flux, peak column density, and angular size can all be described by power laws over a limited range of values. Each of these distributions shows a turnover at low values. For H I flux, the flattening of the slope at $\sim$20 Jy km s^{-1} evident in Figure 11 corresponds to an H I mass, $M_{\rm H\,I} \approx 4.5 D^2_{\rm kpc}\, M_\odot$. This value is consistent with the likely completeness limit noted earlier. Figure 12 shows that the peak column density flattens from a power law below $N_{\rm H\,I} \sim 2 \times 10^{19}$ cm^{-2}. This is slightly higher than the completeness limit noted above of $\sim 10^{19}$ cm^{-2}. Some of the flattening may be real, but a better understanding of the selection limits is needed. The angular size distribution based on the total number of pixels assigned to each cloud is shown in Figure 13. The peak is

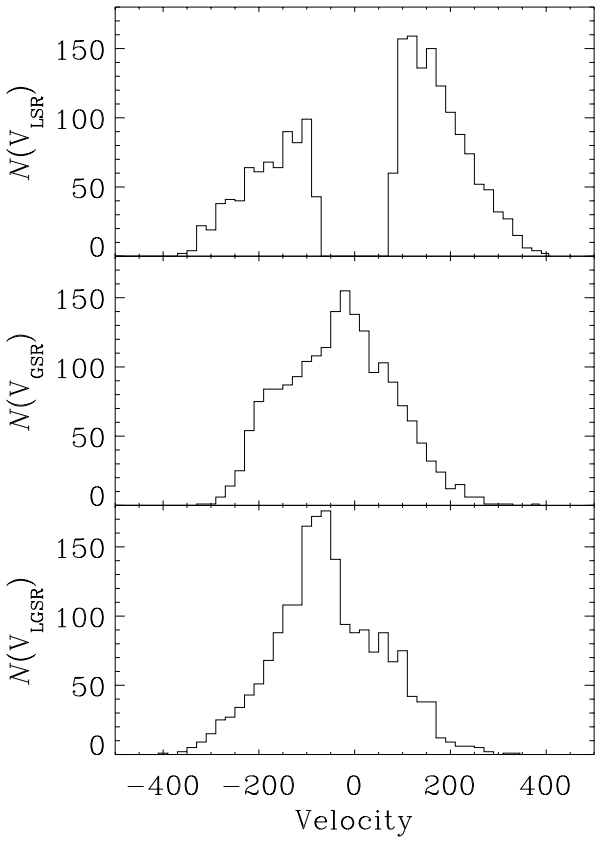

FIG. 10.—Histogram of velocities of all the anomalous-velocity objects identified in the HIPASS data, in three different kinematic reference frames: *top*, with respect to the local standard of rest; *middle*, with respect to the Galactic standard of rest; *bottom*, with respect to the Local Group standard of rest.

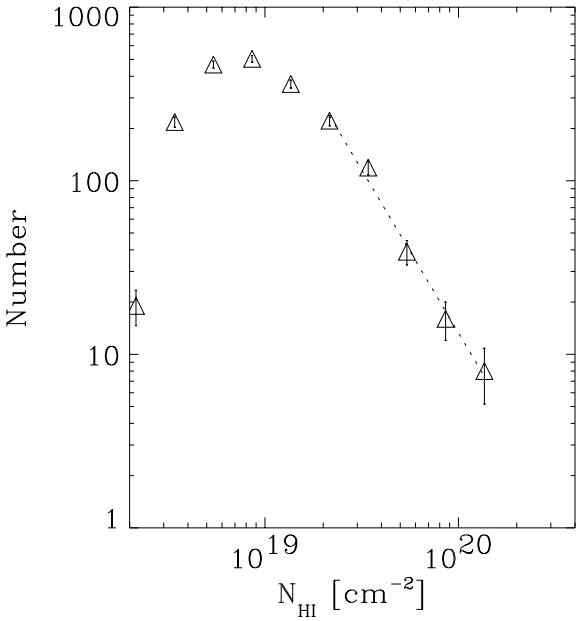

FIG. 12.—Distribution of peak H I column density, $N_{\rm H\ I}$, for all the anomalous-velocity objects cataloged. The data are binned in equal intervals of $\log N_{\rm H\,I}$. The slope of −1.9 implies a distribution function, in linear units, $f(N_{\rm H\,I}) \propto N_{\rm H\,I}^{-2.9}$.

between 0.2 and 0.7 deg^2, which is significantly resolved with the ∼0.07 deg^2 survey resolution. The turnovers seen in all the distributions in the log-log plots of Figures 11–14 appear consistent with the presently understood selection effects inherent in the catalog, making it possible that there exists an underlying power law in the distribution of total flux density, column density, and angular size to lower limits than those probed in the present catalog.

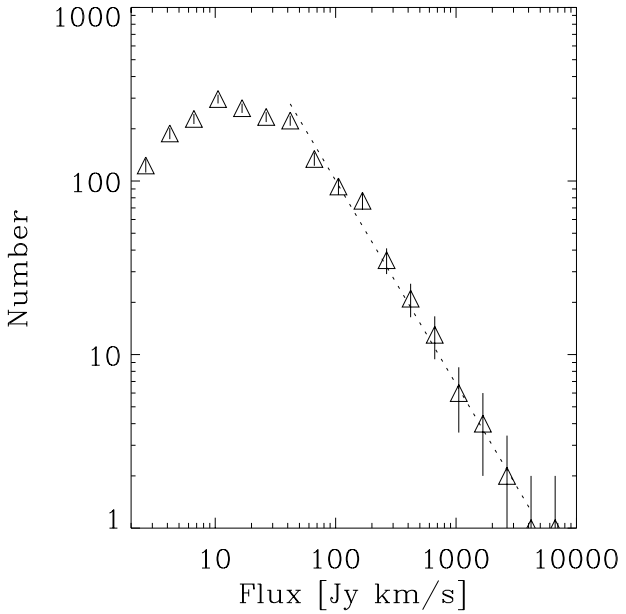

FIG. 11.—Distribution of total H I fluxes, $F_{\rm H\ I}$, for all the anomalous-velocity objects cataloged. The data are binned in equal intervals of $\log F_{\rm H\,I}$. The slope of −1.1 implies a distribution function, in linear units, $f(F_{\rm H\,I}) \propto F_{\rm H\,I}^{-2.1}$.

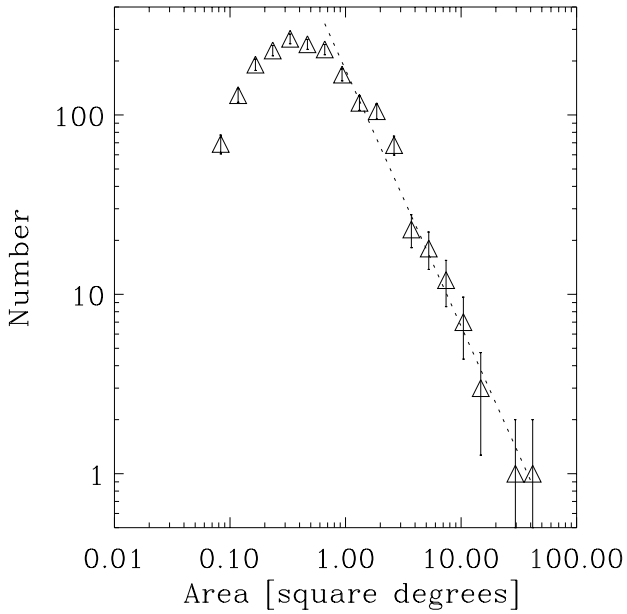

FIG. 13.—Distribution of angular size, θ, for all the anomalous-velocity objects cataloged. The data are binned in equal intervals of $\log \theta$. The distribution is highly peaked between 0.3 and 0.5 deg^2 and implies a distribution function, in linear units, $f(\theta) \propto \theta^{-2.4}$.

The differential H I flux distribution, $f(F_{\rm H\,I}) \propto F_{\rm H\,I}^{-2.1}$ (Fig. 11) has a slope (above 30 Jy km s^{-1}) slightly more negative than the limiting value of -2, below which the total flux becomes dominated by the contribution from the low-flux end. WvW91 obtained a shallower power-law dependence, $f(F_{\rm H\,I}) \propto F_{\rm H\,I}^{-1.5}$, in their discussion of earlier survey data with coarser resolution. The principal reason for this difference is likely to be the qualitative organization of individual objects into larger clouds and complexes, which will populate the high-flux tail of the distribution at the expense of the low-flux peak. If the distance to individual objects were known it would be possible to construct the H I mass distribution function from our data. However, it is possible that the HVC distances span more than 2 orders of magnitude, so we cannot easily constrain the intrinsic mass function shape at this time.

The peak column density distribution function, $f(N_{\rm H\,I}) \propto N_{\rm H\,I}^{-2.9}$, shown in Figure 12, implies that high observed column densities are extremely rare. The distribution turns over near $N_{\rm H\,I} \sim 8 \times 10^{18}$ cm^{-2}, and the median peak column density (Table 2) is 9×10^{18} cm^{-2}. These values may be dependent on the resolution and completeness limits. The median FWHM line width is 36 km s^{-1} with a dispersion of only 12 km s^{-1}, making the distribution in line width effectively single-valued. Since the median is only marginally in excess of the relatively coarse velocity resolution, the measured line width must be regarded as an upper limit.

Figure 13 shows the angular size distribution function, $f(\theta) \propto \theta^{-2.4}$, which peaks between 0.3 and 0.5 deg^2. The median angular size of a cataloged cloud is 0.41 deg^2. The distribution of total sky area covered as a function of cloud area is shown in Figure 14. The majority of sky area coverage by cataloged anomalous-velocity H I is contributed by features between 0.5 and 3 deg^2 in size. The total area of southern sky covered by high-velocity emission features is 1582 deg^2.

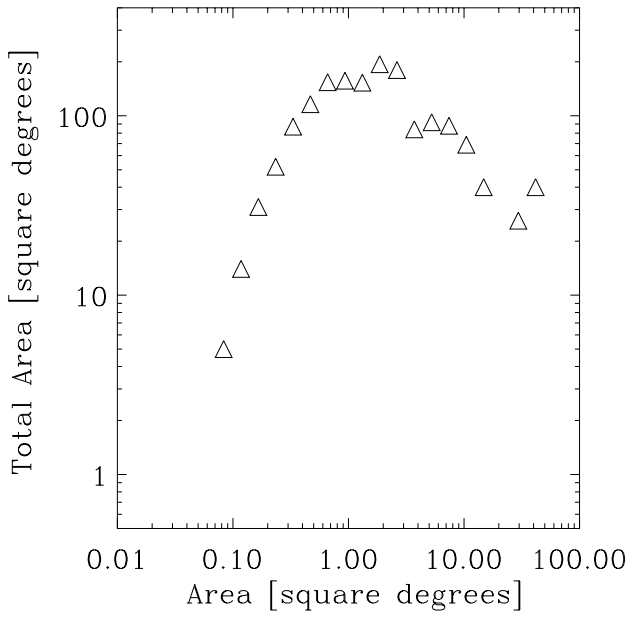

FIG. 14.—Distribution of total sky area covered as a function of cloud area for all the anomalous-velocity objects cataloged. The largest contribution to areal coverage is provided by objects with an angular size of ~2 deg^2. The total area of southern sky covered by high-velocity emission features is 1582 deg^2.

For those objects with a minor-to-major axial ratio less than 0.7 the distribution of position angles of the anomalous objects with respect to Galactic coordinates is shown in Figure 15. The distribution is relatively uniform, with the exception of an enhancement within about 20° of 0°/180°, implying an excess alignment perpendicular to the Galactic plane for about 10% of all cataloged objects. This excess is largely the same population of clouds that follows the general orientation of the Magellanic Stream. Figure 16 shows the distribution of position angles with respect to the Magellanic coordinate system, as defined below. The north pole of these coordinates is defined to lie at Galactic coordinates $(l, b) = (180°, 0°)$; the equator of the Magellanic system, i.e., latitude B_M, forms a great circle passing through the south Galactic pole and through the Galactic equator at $l = 90°$ and 270°. The Magellanic Stream lies roughly parallel to the equator of the Magellanic coordinate system but generally slightly to its south. The zero of Magellanic longitude, $L_M = 0°$, is defined to coincide with the position of the LMC. The peak near 90° in Figure 16 shows an excess of about 10% of cataloged objects to be aligned parallel with the Magellanic Stream.

3.2. *Distribution of the Compact High-Velocity Clouds*

If any of the anomalous-velocity clouds are at Local Group or larger distances, they are likely to be small and distinct from the large high-velocity complexes. We classified 179 of the cataloged objects as compact, isolated CHVCs, following the criteria outlined in § 2.4. A further 159 could not be unambiguously classified as CHVCs and received the :HVC designation. This number is well in excess of the 65 compact, isolated clouds cataloged by BB99 between decl. −30° and 90°. Of the BB99 CHVCs, we find that about 50% in the declination range −30° to 2° do not satisfy the more stringent selection criteria that we have adopted for a CHVC classification in the HIPASS data. With the higher resolution and sensitivity we detected elon-

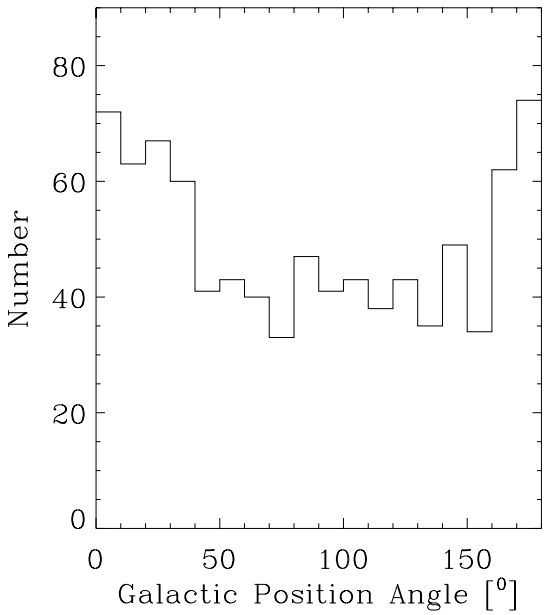

FIG. 15.—Distribution of position angles, with respect to Galactic coordinates, for all the anomalous-velocity objects cataloged.

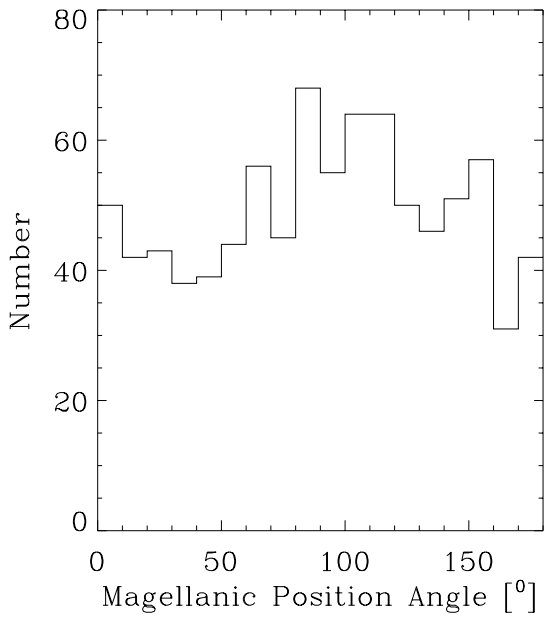

FIG. 16.—Distribution of position angles, with respect to Magellanic coordinates, for all the anomalous-velocity objects cataloged.

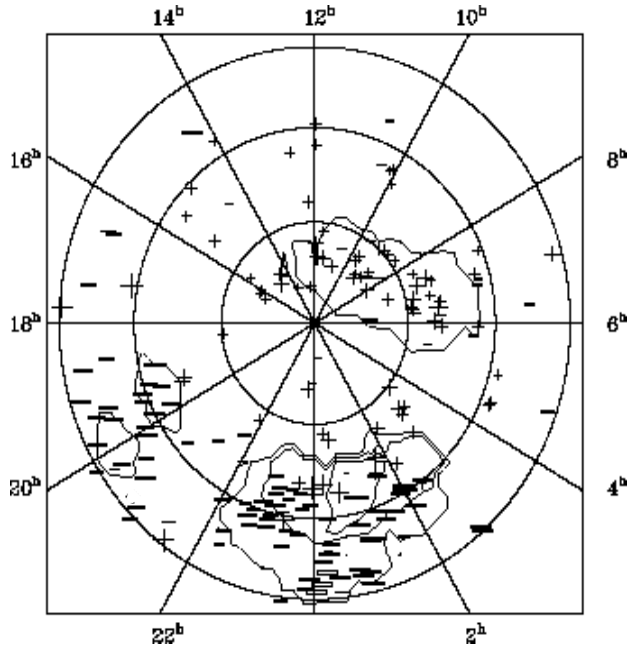

FIG. 17.—Distribution of CHVC objects cataloged in the south polar cap projection. Plus and minus signs are used to indicate positive and negative velocities in the GSR frame, with the size of the sign proportional to magnitude. Contours of local velocity dispersion are drawn at values of 50, 100, and 150 km s^{-1}.

gations at low brightnesses in some cases that make their association with nearby filamentary structures a possibility.

This section describes only the compact and isolated CHVCs cataloged in the HIPASS data. The spatial distribution of the CHVCs is shown in the polar cap projection in Figure 17. The same local minima noted above for the entire anomalous-velocity H I distribution apply here: because of survey incompleteness there is a strong anticorrelation with the Galactic disk, as well as with the Magellanic Clouds. Several apparent concentrations of CHVCs are seen in excess of a more nearly uniform distribution. We will refer to the most prominent concentrations by name: Group 1, extending about $(\alpha, \delta) = (23^h \rightarrow 2^h, 0^\circ \rightarrow -45^\circ)$; Group 2, $(\alpha, \delta) = (6^h \rightarrow 12^h, -45^\circ \rightarrow -70^\circ)$; and Group 3, $(\alpha, \delta) = (19^h \rightarrow 21^h, 0^\circ \rightarrow -35^\circ)$. It must be borne in mind, however, that the appearance of such concentrations will be strongly modified by the variations in survey completeness. In particular, Group 1 is bisected by a bright portion of the Magellanic Stream, while Group 2 is adjacent to a region of extensive Galactic emission, as can be seen by comparison with Figures 3 and 5. The distribution of the compact high-velocity clouds in Galactic coordinates is shown in Figure 18. In Galactic coordinates, the CHVC concentrations fall near the south Galactic pole (Group 1), near $(l, b) = (270^\circ, -15^\circ)$ (Group 2), and near $(l, b) = (10^\circ, -20^\circ)$ (Group 3).

The Group 1 CHVC concentration extends across the Magellanic Stream and is also spatially coextensive with the Sculptor Group of galaxies, though the most prominent CHVC peak is offset from the center of both the Stream and the Sculptor Group. This group of CHVCs has an extreme variation in velocity over a limited region of the sky. We have calculated the velocity dispersion as a function of position on the sky for all CHVCs within a radius of 15°, whenever at least 10 objects fall within this circle. The resulting contours of velocity dispersion are drawn in Figure 17. Peak dispersions of 150 km s^{-1} are found toward Group 1. Though this value is affected by the V_{LSR} cutoff, comparable velocity dispersions are seen nowhere else in the southern sky, nor in the CHVC compilation of BB99. See Putman et al. (2002) and Putman (2000) for a thorough description of this sight line through the Magellanic Stream.

Group 2 is spatially in the region leading the Magellanic Clouds and is also near the Local Group antibarycenter position $(\alpha, \delta) = (11^h, -45^\circ)$, where Blitz et al. (1999) predict an excess of Local Group debris. The velocities of Group 2 are predominantly positive in the LSR frame. Group 3 is the most diffuse of the CHVC concentrations, with only a minor increase in the local number density. This concentration overlaps the region designated the GCN (galactic center negative velocity) complex by WvW91.

The angular two-point correlation function, $w(\theta)$, for CHVCs is significantly positive for separations on the sky with $\theta < 20^\circ$ (Fig. 19), confirming that CHVCs are clustered. The function $w(\theta)$ for all the HVCs is also shown in Figure 19, and they are found to be less clustered than the CHVCs. The function $w(\theta)$ is computed by counting pairwise separations, $N(\theta)$ in the range $(\theta, \theta + d\theta)$ and evaluating

$$w(\theta) = \frac{\rho_r^2 N(\theta)}{\rho^2 N_r(\theta)} - 1\,, \qquad (1)$$

where ρ is the mean cloud density, $N_r(\theta)$ is the number of pairwise separations in a random cloud catalog, and ρ_r is the random cloud density. The random ($n = 10^4$) cloud catalog has identical selection in declination ($<2^\circ$) and excludes Galactic latitudes within $|b| = 10^\circ$ because of the velocity bias against this region in the HVC catalog. The function $w(\theta)$ gives the excess probability, over the Poisson probability, of finding two clouds with separation θ. The random cloud catalog permits correlations arising from the angular selection function to be effectively removed. See Hamilton

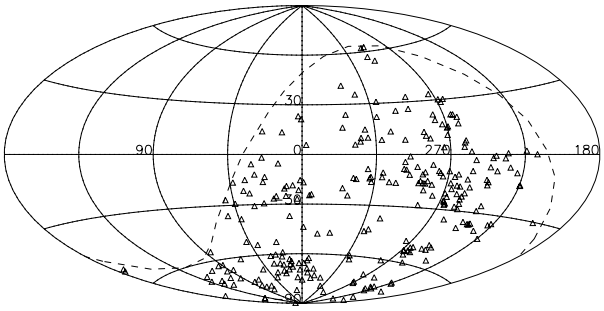

FIG. 18.—Distribution of the compact high-velocity clouds (CHVCs) in Galactic coordinates.

(1993) for a discussion of correlation functions and estimators. For CHVCs, $w(\theta)$ appears to be approximated by a power law with $w(\theta) = (\theta/10^\circ)^{-0.6}$. For HVCs, the slope is similar but is better defined, with $w(\theta) = (\theta/2^\circ)^{-0.8}$. CHVCs are significantly more clustered than HVCs. In the range $2^\circ < \theta < 20^\circ$, CHVCs have twice the excess probability of being paired, compared with HVCs.

The velocity distribution of the cataloged CHVCs is plotted against Galactic longitude and latitude in Figures 20 and 21, respectively, for the Local, Galactic, and Local Group reference frames. The velocity histograms in these reference frames are shown in Figure 22. Comparison of the CHVC velocity distributions with those of all the clouds suggests that the CHVCs are more nearly equally distributed between positive and negative LSR velocities. In the GSR frame, the prominent peak at $V_{\rm GSR} = -30$ km s^{-1} in Figure 10 is not seen in the CHVC distribution shown in Figure 22. The velocity distribution of the CHVCs declines from a dispersion of 125 km s^{-1} in the GSR frame to 116 km s^{-1} in the LGSR frame. The high positive velocity tail in the LGSR distribution of the CHVCs is contributed to a large extent by the objects of Group 1. Table 2 shows that the median LSR, GSR, and LGSR velocities (95, -38, and -57 km s^{-1}, respectively) are only slightly different from the other cloud populations. The mean velocities are 12 (LSR), -47 (GSR), and -56 km s^{-1} (LGSR).

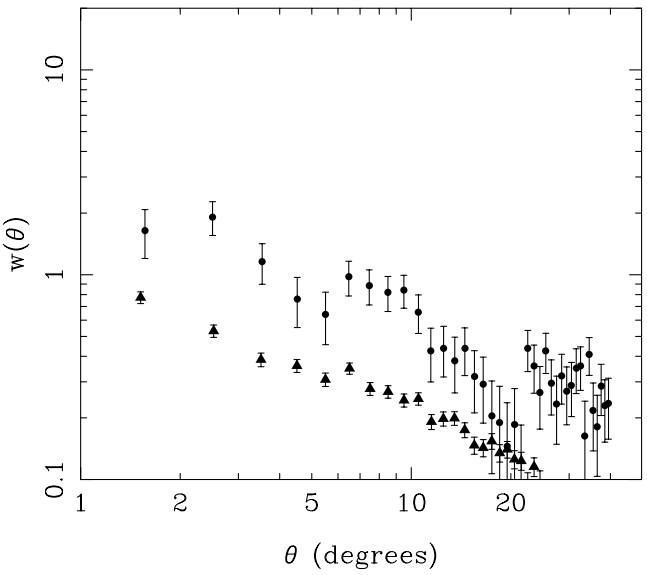

FIG. 19.—Angular two-point correlation function, $w(\theta)$, for HVCs (*triangles*), and CHVCs (*circles*).

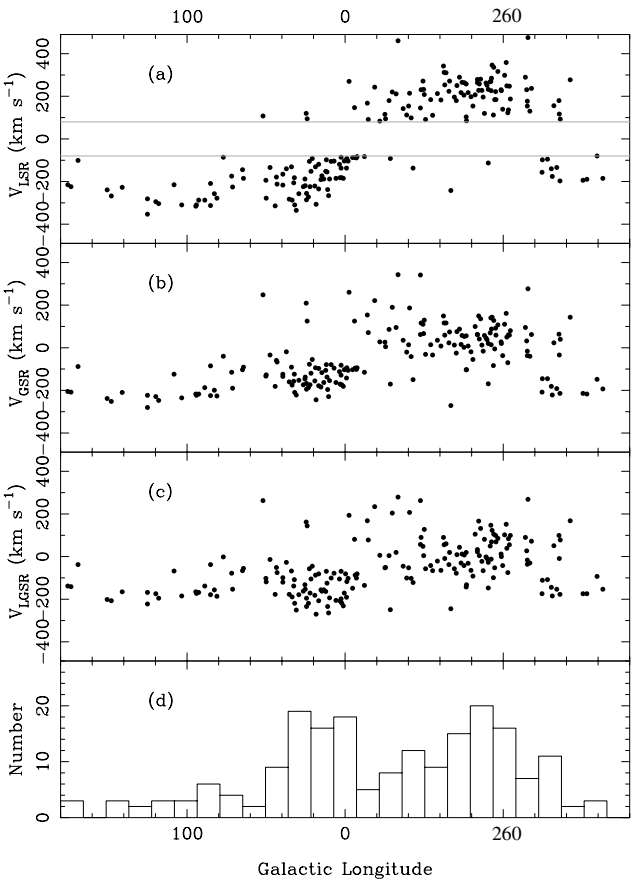

FIG. 20.—Velocities of CHVC objects identified in the HIPASS data, plotted against Galactic longitude for three different kinematic reference frames: (*a*) with respect to the local standard of rest; (*b*) with respect to the Galactic standard of rest; (*c*) with respect to the Local Group standard of rest. (*d*) Number of compact high-velocity clouds in terms of Galactic longitude.

The distributions of CHVC fluxes, peak column densities, and sizes are shown in the log-log plots of Figures 23, 24, and 25, respectively. Steep distributions are found with low-end turnovers that are consistent with the survey completeness limits. Flattening of the flux distribution from the form $f(F_{\rm H\,I}) \propto F_{\rm H\,I}^{-2.1}$ begins at $\sim$30 Jy km s^{-1}, while the peak column density distribution begins to flatten from $f(N_{\rm H\,I}) \propto N_{\rm H\,I}^{-2.8}$ near 2×10^{19} cm^{-2}. The peak in the size distribution, $f(\theta) \propto \theta^{-2.5}$, is at $\sim$0.3 deg^2, which corresponds to significantly resolved sources. Plotting total sky area covered as a function of cloud area in Figure 26 reveals that most of the observed CHVC covering factor is indeed due to resolved objects with a characteristic size of about 0.5 deg^2. The total sky area covered by the southern CHVCs is 85 deg^2, with the largest contributors being CHVCs with sizes between 0.4 and 1 deg^2.

Table 2 shows that the CHVCs have a higher median total flux and peak column density than the entire anomalous-velocity cloud sample. This may be largely due to the selection criteria for a CHVC requiring a peak column density greater than 12 σ. The median size for a CHVC is 0.36 deg^2, which is only slightly smaller than the median size of a cataloged HVC (0.42 deg^2), despite the 2° upper limit to angular size in their selection. Therefore, the main distinguishing

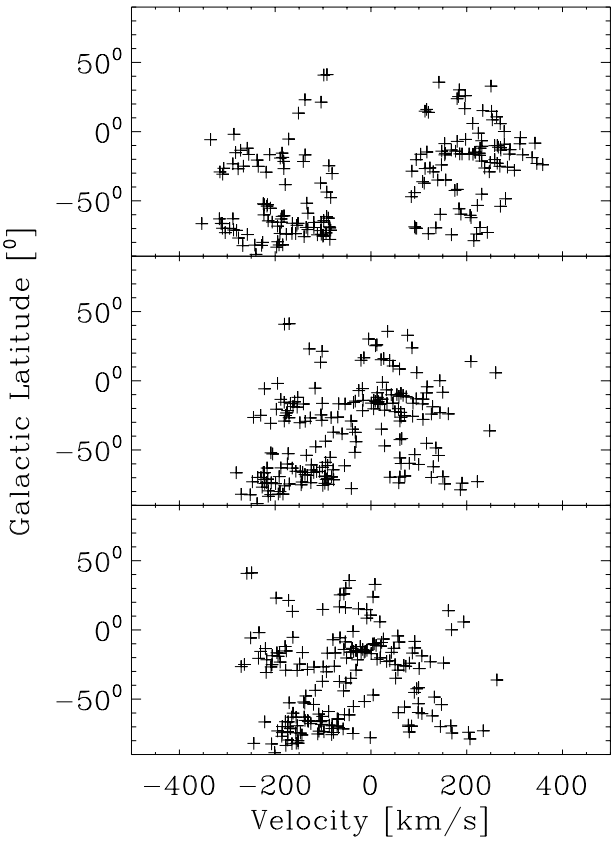

FIG. 21.—Galactic latitude vs. velocities of CHVC objects identified in the HIPASS data, in three different kinematic reference frames: *top*, with respect to the local standard of rest; *middle*, with respect to the Galactic standard of rest; *bottom*, with respect to the Local Group standard of rest.

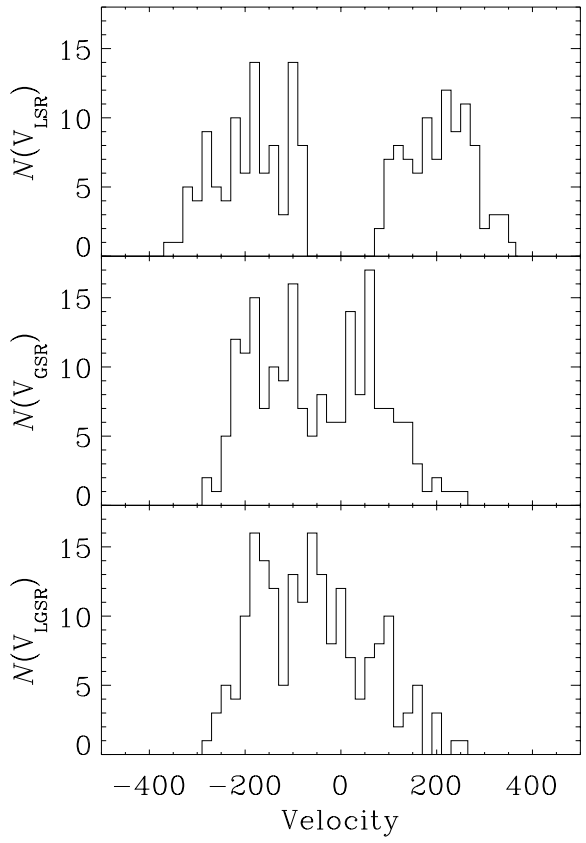

FIG. 22.—Histogram of velocities of CHVC objects identified in the HIPASS data, in three different kinematic reference frames: *top*, with respect to the local standard of rest; *middle*, with respect to the Galactic standard of rest; *bottom*, with respect to the Local Group standard of rest.

feature of HIPASS CHVCs is isolation, rather than compactness. The properties of the CHVCs were investigated in terms of Galactic coordinates and no gradient in individual total flux with position was found. This also holds for the peak column densities and sizes. By definition, the CHVCs do not have a preference for a specific position angle. The :HVCs also do not have a preferred position angle.

4. DISCUSSION AND SUMMARY

The high resolution and sensitivity of HIPASS, combined with repeated coverages that together yield Nyquist sampling and source confirmation have provided an unprecedented view of anomalous-velocity H I emission in the southern hemisphere. These attributes make it possible to detect the morphology of emission features and utilize this in their classification, rather than relying only on their position and velocity. The majority of emission features are associated with relatively diffuse filaments with modest variations in surface brightness. In addition to an assortment of filamentary complexes, there is also a distinct population of compact, isolated objects with a high column density contrast, the CHVCs. The superior resolution and sensitivity of the HIPASS data have allowed much better discrimination of CHVC and HVC sources than was possible previously.

4.1. *HVCs*

As is evident from a comparison of Figures 3 to 5 with Figure 6, the southern sky is rich in anomalous-velocity H I.

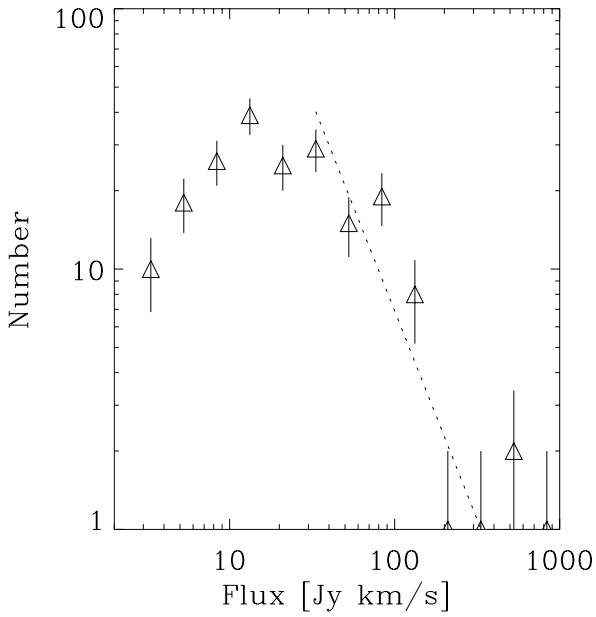

FIG. 23.—Distribution of total H I fluxes, $F_{\rm H\,I}$, for the CHVCs cataloged. The data are binned in equal intervals of $\log F_{\rm H\,I}$. The slope of -1.1 implies a distribution function, in linear units, $f(F_{\rm H\,I}) \propto F_{\rm H\,I}^{-2.1}$.

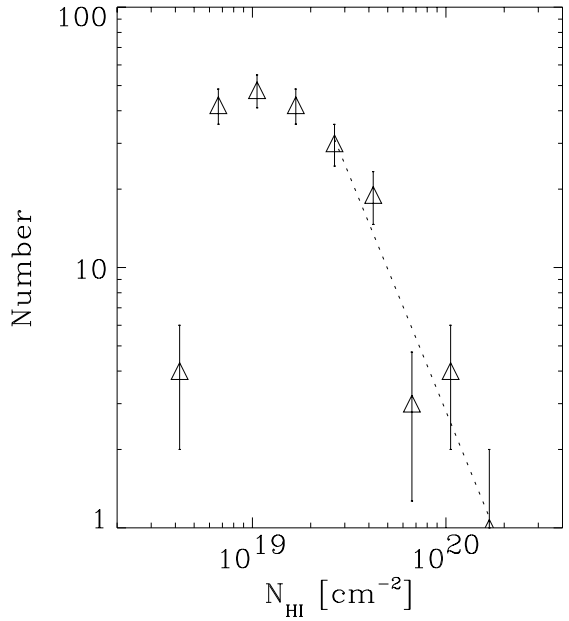

FIG. 24.—Distribution of peak H I column density, $N_{\rm H\,I}$, for the CHVCs cataloged. The data are binned in equal intervals of $\log N_{\rm H\,I}$. The slope of -1.8 implies a distribution function, in linear units, $f(N_{\rm H\,I}) \propto N_{\rm H\,I}^{-2.8}$.

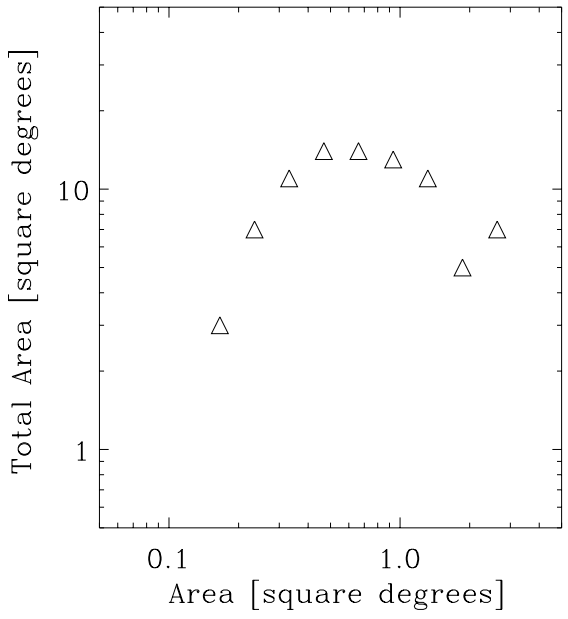

FIG. 26.—Distribution of total sky area covered as a function of cloud area for the CHVCs cataloged. The total sky area covered by the southern CHVCs is 85 $\deg^2$.

The total flux of these objects is dominated by the Magellanic Stream, which accounts for approximately 2.1×10^8 $M_\odot$ of neutral hydrogen (at an average distance of 55 kpc) and is discussed in detail by Putman et al. (2002) and Putman (2000). Also evident from these figures is the perceived avoidance by the anomalous-velocity objects of the Galactic disk and the Magellanic Clouds, largely due to a variable degree of survey completeness resulting from confusion with regions of bright emission extending over a wide range of velocities. One of the most striking features of the spatial distribution is the paucity of anomalous-velocity H I in a region (unaffected by variable completeness) bounded approximately by $(\alpha, \delta) = (2^{\rm h} \rightarrow 5^{\rm h}, -10^\circ \rightarrow -30^\circ)$. In Galactic coordinates, this is centered at $(l, b) \approx (200^\circ, -50^\circ)$, which is both well off the Galactic plane and along a sight line that extends over only one spiral arm (see Taylor & Cordes 1993). The percentage of our Galaxy that lies along a particular sight line may have implications on the number of HVCs in that direction.

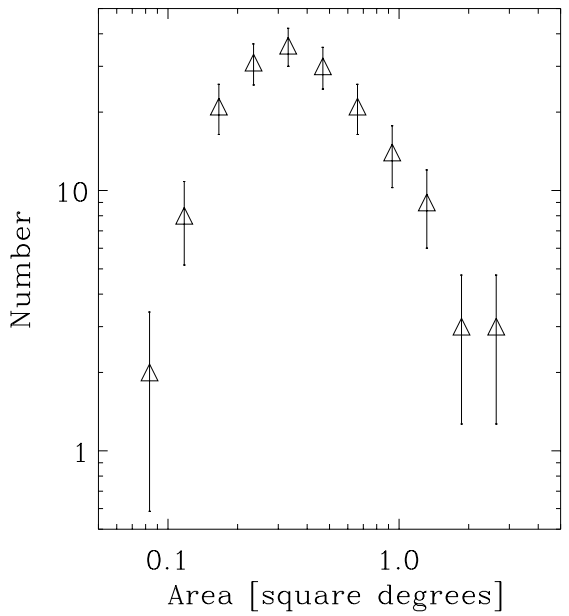

FIG. 25.—Distribution of angular size, θ, for the CHVCs cataloged. The data are binned in equal intervals of $\log \theta$. The distribution is highly peaked between 0.3 and 0.4 $\deg^2$ and implies a distribution function, in linear units, $f(\theta) \propto \theta^{-2.5}$ (or $\theta^{-2.2}$ if the last two points are excluded from the fit).

The distributions of total flux and peak column density for the entire population of cataloged anomalous-velocity clouds can be described by steep power laws (of slopes -2.1 and -2.9, respectively) with a flattening at low values due to the nominal survey completeness limit. The distribution of apparent cloud sizes is strongly peaked at angular sizes in the range 0.3–0.5 $\deg^2$. These properties imply that the majority of cataloged objects share a characteristic flux, $\sim$20 Jy km s^{-1}; peak column density, $\sim 10^{19}$ cm^{-2}; and size, $\sim$0.4 $\deg^2$, in agreement with the median properties listed in Table 2. Unless the clouds can be assigned a characteristic distance, the distribution of total flux cannot be easily converted into an H I mass function of anomalous-velocity gas. If one assumes a characteristic distance, D, the mass of a typical cloud is $\sim 4.5 D_{\rm kpc}^2\, M_\odot$.

The distribution of position angles of the high-velocity clouds indicates that an excess of about 10% is aligned along the long axis of the Magellanic Stream and may have a common origin. A comparable excess of objects is found elongated perpendicular to the Galactic plane, although this is basically the same population of objects, given the orientation of the Stream. This excess remains when the narrow region of sky traditionally associated with the Magellanic Stream is excluded from the analysis. The elongation of the clouds may represent an interaction with material in the Galactic halo or the strength of the gravitational field of the Milky Way. Quilis & Moore (2001) find that head-tail

features in HVCs (similar to the :HVC pictured in Fig. 2) can be reproduced either in pure gas clouds or in clouds embedded in dark matter halos, as long as the Galactic wind density is higher than 10^{-4} cm^{-3}. They suggest that all HVCs will show tails with higher sensitivity observations. The reclassification of many of the BB99 CHVCs due to detection of low column density extensions from the cloud cores with HIPASS may represent the detection of these tails.

Based on the completeness levels of the catalog (see § 2.5), high-velocity features cover 19% of the southern sky. This is almost exactly the value found by Wakker (1991) for $|V_{\rm LSR}| > 100$ km s^{-1} and $N_{\rm H\,I} > 2 \times 10^{18}$ cm^{-2} by using the WvW91 all-sky catalog. Murphy, Lockman, & Savage (1995) found a covering fraction of 37% in the regions around active galactic nuclei for $N_{\rm H\,I} > 7 \times 10^{17}$ cm^{-2}. This covering fraction agrees with the extrapolation of $N_{\rm H\,I}$ down to this level in the all-sky surveys (Wakker 1991). The detection of high-velocity O VI and Mg II absorption lines (Sembach et al. 2000; Gibson et al. 2000) and Hα emission (Tufte, Reynolds, & Haffner 1998) off the 21 cm survey contours also suggests a larger all-sky covering fraction for high-velocity gas. The high-velocity cloud features presented here may simply be the high H I column density peaks among a dense web of multiphase halo material.

The peak column density distribution of the anomalous-velocity clouds is significantly steeper than the distribution of column densities observed in quasar absorption lines (Penton et al. 2000; Hu et al. 1995) and (for $N_{\rm H\,I} < 10^{21}$ cm^{-2}) the galaxies of the Ursa Major cluster (Zwaan, Verheijen, & Briggs 1999). These comparisons may be premature since we are sampling the distribution of peak cloud column densities rather than the distribution of all column densities. One would have to assume that the decreasing radial distribution that will dominate the surface area and hence the statistics for random sight lines behaves similarly for all clouds. Steps have been taken recently to quantify the radial distributions of column density at the edges of CHVCs (Burton, Braun, & Chengalur 2001). Approximately exponential edge profiles have been observed for $N_{\rm H\,I}$ between a few times 10^{17} and about 10^{19} cm^{-2}, although the scale lengths vary among objects by at least a factor of 5. Also, high-resolution studies of HVCs (e.g., Wakker & Schwarz 1991; Braun & Burton 2000) have shown great variation in column densities within cloud substructures, down to at least arcminute scales. In practice, the variation in apparent peak column density observed with 15′.5 versus 1′ resolution amounts to a factor of about 3 for the HVC complexes A, L, and M, and ranges between a factor of 5 and 20 for the CHVCs that have been studied to date.

Some parallels can be made between those HVCs not directly associated with the Magellanic System (e.g., not the Stream, Leading Arm, and Bridge) and the anomalous-velocity gas seen in NGC 2403 by Sancisi et al. (2001). The anomalous-velocity components of NGC 2403 make up 10% of its total H I mass, with individual long filaments having masses of $\sim 10^6$ and 10^7 $M_\odot$. At a mean distance of 15 kpc, the non-Magellanic HVCs would be ~10% of the Galaxy's H I mass, and the mass estimates for some of the large high-velocity complexes with distance constraints are $\sim 10^6$ $M_\odot$ (complexes A and C; van Woerden et al. 1999; Wakker et al. 1999). Further parallels can be made when one considers that some low $V_{\rm GSR}$ HVCs show clear links to Galactic H I when examined in both position and velocity (e.g., Fig. 6 in Putman & Gibson 1999), and much of the extreme positive and negative high-velocity gas can be associated with the Magellanic HVCs. The XHVCs listed in Table 3 merge with Galactic emission, and though some may simply lie at overlapping velocities, they have a higher likelihood of being directly related to the Galaxy. Further deep H I studies of Milky Way–like spirals will provide important insight into the nature of the anomalous-velocity gas that surrounds our Galaxy.

4.2. *CHVCs*

We have cataloged a substantial population (179) of compact, isolated high-velocity H I clouds (CHVCs) in the southern hemisphere as shown in Figure 17. The quality of the HIPASS data has resulted in this sample being larger than the sample of 65 objects north of decl. $-30°$ cataloged by BB99, despite the fact that we have applied more stringent selection criteria. For our HIPASS sample we have demanded that the 25% column density contour of each object (1) be closed, with a diameter less than 2°, (2) not be elongated in the direction of any nearby extended emission, and (3) be well above the local noise floor (implying a peak signal-to-noise ratio of at least 12 σ). By comparison, BB99 applied the same three criteria to the 50% column density contour seen in the LDS data. Only 50% of the BB99 CHVC sample in the declination zone of overlap satisfy these more demanding conditions in the HIPASS data. These results suggest that the CHVC classification is dependent on the sensitivity and resolution of the survey used to classify them; however, the increase in the number of cataloged CHVCs could also partially be due to a bias in their overall distribution for the southern hemisphere. In a subsequent paper (de Heij et al. 2002) the Leiden-Dwingeloo database is investigated with the same search algorithm and selection criteria employed here.

The distribution of cataloged southern CHVCs is not uniform on the sky. The angular two-point correlation function of CHVCs, shown in Figure 19, suggests that they are approximately twice as clustered as the more general HVC population, out to angular scales of about 20°. There are several possible reasons for the clustering. It may be partially a selection effect due to diminished sensitivity in certain regions of the sky (as discussed in § 2.5). The clustering could also reflect the formation or destruction process of a larger cloud. Finally, CHVCs could represent high column density peaks within a more diffuse medium, similar to what is proposed for galaxies and the Lyα absorber systems, which also appear clustered (Dave et al. 1999). This scenario could also explain the diffuse tails seen around many of the CHVCs and :HVCs (see also the results of Brüns et al. 2000 and Burton et al. 2001). However, as stated in the previous section, the elongation of these clouds could also represent interaction with the Galaxy's halo.

The CHVCs cluster in several concentrations, which we have designated Groups 1, 2, and 3. Group 1 is spatially coextensive with a portion of the Magellanic Stream and the Sculptor Group of galaxies near the south Galactic pole (see Putman et al. 2002; Putman 2000). Kinematically, the distribution extends continuously from the systemic velocity of Sculptor, near $V_{\rm GSR} = +200$ km s^{-1}, to high negative velocities, $V_{\rm GSR} = -300$ km s^{-1}, but it is unknown what the distribution does between -60 km s^{-1} $< V_{\rm dev} <$ 60 km s^{-1}, where there is confusion with Galactic emission. The Magel-

lanic Stream is on the negative velocity side of this undetectable range in this part of the sky. Since this concentration lies near the Galactic pole, the corresponding velocities in the LSR, GSR, and LGSR frames are virtually identical. This kinematic range of 500 km s^{-1} is responsible for a local peak in the velocity dispersion of CHVC objects, which is not seen anywhere else in the southern sky (see Fig. 17). The Group 2 concentration of CHVCs is a more diffuse collection of objects with high positive LSR velocities (which have a mean near 0 km s^{-1} in both the GSR and LGSR frames). As noted previously, this concentration is in the Local Group antibarycenter region and also the area leading the Magellanic Clouds; however, it also lies next to the Galactic plane, so the apparent distribution may be strongly affected by confusion effects. A third diffuse concentration of CHVCs, Group 3, is characterized by high negative velocities in the both the LSR and GSR frames.

If one presumes that CHVCs are self-gravitating gas clouds, their distance can be estimated from the virial theorem by using

$$D_{\rm vir} = f\,\frac{3\sigma^2\sqrt{\Omega}}{2\sqrt{\pi}G0.236F_{\rm H\,I}} \qquad (2)$$

(following Wakker et al. 2002), where f is $M(\mathrm{H\,I})/M(\mathrm{total})$, σ is the velocity dispersion in kpc Myr^{-2} [$=\sigma$ (km s^{-1}) $\times 1.023 \times 10^{-3}$], Ω is the solid angle of the CHVC, $G = 4.53 \times 10^{-12}$ kpc^3 Myr^{-2} $M_\odot^{-1}$, and $F_{\rm H\,I}$ is the H I flux in jansky-kilometers per second. The median angular size, Ω, of a HIPASS CHVC is 0.36 deg^2, the velocity dispersion, σ, is typically 10–15 km s^{-1}, and the median total flux, $F_{\rm H\,I}$, is 19.9 Jy km s^{-1}. If $f = 0.1$, the CHVCs are at a median distance, $D_{\rm vir}$, of 400 kpc. With an estimate of a CHVC's distance, the total flux can be thought of in terms of its H I mass by using $M_{\rm H\,I} = 0.236F_{\rm H\,I}D_{\rm kpc}^2\ M_\odot$, where $F_{\rm H\,I}$ is in jansky-kilometers per second. At a distance of 400 kpc, the entire population of CHVCs has a range of H I masses from 3.8×10^4 to $3.4 \times 10^7\ M_\odot$, with a median value of $7.5 \times 10^5\ M_\odot$. Moving the clouds out to 700 kpc ($f = 0.3$) gives a median H I mass of $2.3 \times 10^6\ M_\odot$, and 55 kpc ($f = 0.02$) gives $1.4 \times 10^4\ M_\odot$. The actual value of $M(\mathrm{H\,I})/M(\mathrm{total})$ and whether or not CHVCs are self-gravitating remain to be determined. If CHVCs are not self-gravitating and there is no other confining medium, the clouds are unlikely to last more than a few hundred million years (again depending on the cloud's distance; e.g., see Blitz et al. 1999). Using the classic crossing-time argument, at 55 kpc a typical CHVC would double in size in only 25 Myr.

The distribution of CHVC sizes has a slightly steeper slope than the entire population of clouds, probably because of the 2° upper size limit imposed in the catalog. CHVCs cover only 1% of the southern sky. The CHVC distributions of flux and peak column density have approximately the same slope as the entire population of HVCs. So again, the $N_{\rm H\,I}$ slope is steeper than that of a sample of galaxies. The $F_{\rm H\,I}$ slope is actually shallower than that of a sample of galaxies taken from the HIPASS survey [$f(F_{\rm H\,I}) \propto F_{\rm H\,I}^{-2.7}$; Kilborn 2000; Putman 2000]. There is no systematic distribution of cloud fluxes and sizes with velocity or position that could be used to argue for a greater distance in certain regions of the sky or at higher velocities. CHVCs have a median GSR velocity of -38 km s^{-1}, which is suggestive of infall and is similar to the northern population of CHVCs (BB99). The median and mean LGSR velocity is slightly lower for the CHVCs than the other populations of clouds.

We are grateful to Mark Calabretta for his help in developing the software for reducing HIPASS. M. Putman thanks the Australia Telescope National Facility for hosting her during much of this work and Zonta International for travel funding. Swinburne University is thanked for the use of their supercomputing facility. The Netherlands Foundation for Research in Astronomy is operated under contract with the Netherlands Organization for Scientific Research. This research has made use of the NASA/IPAC Extragalactic Database (NED), which is operated by the Jet Propulsion Laboratory, California Institute of Technology, under contract with the National Aeronautics and Space Administration. We have also made use of the LEDA database (see http://leda.univ-lyon1.fr). The Digitized Sky Surveys were produced at the Space Telescope Science Institute under government grant NAG W-2166.

REFERENCES

Bajaja, E., Morras, R., & Pöppel, W. G. L. 1987, Publ. Astron. Inst. Czechoslovakia Acad. Sci., 69, 237
Barnes, D. G., et al. 2001, MNRAS, 322, 486
Blitz, L., Spergel, D. N., Teuben, P. J., Hartmann, D., & Burton, W. B. 1999, ApJ, 514, 818
Braun, R., & Burton, W. B. 1999, A&A, 341, 437 (BB99)
———. 2000, A&A, 354, 853
Brüns, C., Kerp, J., Kalberla, P. M. W., & Mebold, U. 2000, A&A, 357, 120
Burton, W. B. 1988, in Galactic & Extragalactic Radio Astronomy, ed. G. L. Verschuur & K. I. Kellermann (Berlin: Springer), 295
Burton, W. B., Braun, R., & Chengalur, J. N. 2001, A&A, 375, 219
Dave, R., Hernquist, L., Katz, N., & Weinberg, D. H. 1999, ApJ, 511, 521
de Heij, V., Braun, R., & Burton, W. B. 2002, A&A, in preparation
Eichler, D. 1976, ApJ, 208, 694
Einasto, J., Haud, U., Jôeveer, M., & Kaasik, A. 1976, MNRAS, 177, 357
Gibson, B. K., Giroux, M. L., Penton, S. V., Putman, M. E., Stocke, J. T., & Shull, J. M. 2000, AJ, 120, 1830
Giovanelli, R. 1981, AJ, 86, 1468
Gnedin, N. Y. 2000, ApJ, 542, 535
Hamilton, A. J. S. 1993, ApJ, 417, 19
Hartmann, D., & Burton, W. B. 1997, Atlas of Galactic Neutral Hydrogen (Cambridge: Cambridge Univ. Press)
Henning, P. A., Rivers, A. J., & Staveley-Smith, L. 2000, in ASP Conf. Ser. 218, Mapping the Hidden Universe, ed. R. C. Kraan-Korteweg, P. A. Henning, & H. Andernach (San Francisco: ASP), 61
Henning, P. A., Kraan-Korteweg, R. C., Rivers, A. J., Loan, A. J., Lahav, O., & Burton, W. B. 1998, AJ, 115, 584
Henning, P. A., et al. 2002, AJ, in press
Hu, E. M., Kim, T.-S., Cowie, L. L., Songaila, A., & Rauch, M. 1995, AJ, 110, 1526
Hulsbosch, A. N. M. 1968, Bull. Astron. Inst. Netherlands, 20, 33
Kilborn, V. 2000, Ph.D. thesis, Univ. Melbourne
Kilborn, V., Webster, R. L., & Staveley-Smith, L. 1999, Publ. Astron. Soc. Australia, 16, 8
Klypin, A., Kravtsov, A. V., Valenzuela, O., & Prada, F. 1999, ApJ, 522, 82
Koribalski, B. et al. 2002, in preparation
Mirabel, I. F., & Franco, M. L. 1976, Ap&SS, 39, 415
Moore, B., Ghigna, S., Governato, G., Lake, G., Quinn, T., Stadel, J., & Tozzi, P. 1999, ApJ, 524, L19
Morras, R., Bajaja, E., Arnal, E. M., & Pöppel, W. G. L. 2000, A&AS, 142, 25
Mulchaey, J. S. 2000, ARA&A, 38, 289
Murphy, E. M., Lockman, F., & Savage, B. D. 1995, ApJ, 447, 642
Oort, J. H. 1966, Bull. Astron. Inst. Netherlands, 18, 421
———. 1968, in IAU Symp. 29, Non-stable Phenomena in Galaxies, ed. A. Arakelyan (San Francisco: ASP), 41
———. 1970, A&A, 7, 381
———. 1981, A&A, 94, 359
Penton, S. V., Shull, J. M., & Stocke, J. T. 2000, ApJ, 544, 150
Putman, M. E. 2000, Ph.D. thesis, Australian National Univ.
Putman, M. E., & Gibson B. K. 1999, Publ. Astron. Soc. Australia, 16, 70
Putman, M. E., et al. 1998, Nature, 394, 752

Putman, M. E., Staveley-Smith, L., Freeman, K. C., Gibson, B. K., & Barnes, D. G. 2002, in preparation
Quilis, V., & Moore, B. 2001, ApJ, 555, L95
Rees, M. J. 1986, MNRAS, 218, L25
Rivers, A. J. 2000, Ph.D. thesis, Univ. New Mexico Albuquerque
Sancisi, R., Fraternali, F., Oosterloo, T., & van Moorsel, G. 2001, in ASP Conf. Ser. 240, Gas and Galaxy Evolution, ed. J. E. Hibbard, M. Rupen, & J. H. van Gorkum (San Francisco: ASP), 241
Saraber, M. J. M., & Shane, W. W. 1974, A&A, 36, 365
Schneider S. E., & Rosenberg J. L. 2000, in ASP Conf. Ser. 218, Mapping the Hidden Universe, ed. R. C. Kraan-Karteweg, P. A. Henning, & H. Andernach (San Francisco: ASP), 271
Sembach, K. R., et al. 2000, ApJ, 538, L31
Stoppelenburg, P. S., Schwarz, U. J., & van Woerden, H. 1998, A&A, 338, 200
Taylor, J. H., & Cordes, J. M. 1993, ApJ, 411, 674
Tufte, S. L., Reynolds, R. J., & Haffner, L. M. 1998, ApJ, 504, 773
van Woerden, H., Schwarz, U. J., Peletier, R. F., Wakker, B. P., & Kalberla, P. M. W. 1999, Nature, 400, 138
Verschuur, G. L. 1975, ARA&A, 13, 257
Wakker, B. P. 1991, A&A, 250, 499
Wakker, B. P., et al. 1999, Nature, 402, 388
Wakker, B. P., Kalberla, P. M. W., van Woerden, H., de Boer, K. S., & Putman, M. E. 2001, ApJS, 136, 537
Wakker, B. P., Oosterloo, T., & Putman, M. E. 2002, ApJ, in press
Wakker, B. P., & Schwarz, U. 1991, A&A, 250, 484
Wakker, B. P., & van Woerden, H. 1991, A&A, 250, 509 (WvW91)
———. 1997, ARA&A, 35, 217
Wannier, P., & Wrixon, G. T. 1972, ApJ, 173, L119
Wannier, P., Wrixon, G. T., & Wilson, R. W. 1972, A&A, 18, 224
Zwaan, M. A., Verheijen, M. A. W., & Briggs, F. H. 1999, Publ. Astron. Soc. Australia, 16, 100